# Inter-beam Interference Cancellation by 3D Polarized Beamforming in Power Domain NOMA Systems


Author

Nkurunziza Pascal
MC201611

Supervisor

Dr. Xin Su

COLLEGE OF INTERNET OF THINGS ENGINEERING
INFORMATION AND COMMUNICATION ENGINEERING
HOHAI UNIVERSITY

June 2018

# Inter-beam Interference Cancellation by 3D Polarized Beamforming in Power Domain NOMA Systems

Author:

Nkurunziza Pascal

MC201611

A thesis submitted in partial fulfillment of the requirements for the degree of

Master of Science in Information and Communication Engineering

Thesis Supervisor:

Dr. Xin Su

External Examiner Signature:_____

Thesis Supervisor Signature: _____

COLLEGE OF INTERNET OF THINGS ENGINEERING
INFORMATION AND COMMUNICATION ENGINEERING

# ABSTRACT

Inter-beam Interference Cancellation by 3D Polarized Beamforming in Power Domain NOMA Systems

Nkurunziza Pascal

MC201611

Master of Science

Hohai University

2018

The application of beamforming (BF) techniques in power domain non-orthogonal multiple access (NOMA) schemes allows users to share the same single BF vector for operational reliability. The occurrence of inter-beam interference (IBI) is highly probable in a congested cell (i.e., a cell with high user density and active users). IBI cancellation by using 3D polarized BF in order to enhance the practicability of NOMA systems is the focus of this thesis. An IBI cancellation scheme is proposed and evaluations of the spectrum efficiency according to the scenario congestion, as well as of the interference reduction by narrowing the generated beam to a desired beam-width, are presented.

**Keywords:** 3D polarized beamforming, HPBW, IBI cancellation, spectrum efficiency, energy efficiency

# UNDERTAKING

I certify that research work titled "*Inter-beam Interference by 3D Polarized Beamforming in Power Domain NOMA Systems*" is my own work. The work has not been presented elsewhere for assessment. Where material has been used from other sources it has been properly acknowledged/referred.

Signature of Student

Name of Student

Nkurunziza Pascal

MC201611

# ACKNOWLEDGEMENTS

This master's thesis would not have been completed without the Almighty's grace and provision. Deep thanks are addressed to my supervisor, Dr. Xin Su, for his support and guidance. My deepest gratitude is addressed to my supervisor for his excellent guidance along research activities. His extraordinary and unlimited zeal and enthusiasm have been driving forces for bringing me to the research area of wireless communications during my master program.

Many thanks to the School of International Students of Hohai University and the whole university community for their funding support and comfort throughout my master program. I would also like to thank my colleagues in Information and Communication Engineering, Mechanical Engineering; and all my dear friends at Hohai University.

My thanks are as well addressed to the University of Rwanda for having sustained the agreement up to the completion of my program.

Finally, I'm thankful to my brothers and sisters whose love and care unceasingly made my life successful from childhood. Their persistency and selfless support helped me make more progress for several years.

# TABLE OF CONTENTS

# LIST OF FIGURES

# LIST OF TABLES

# LIST OF ABBREVIATIONS

**1-D LSE:** One-dimensional Least Square Estimator

**2-D WFE:** Two-dimensional Wiener Filter Estimator

**3GPP:** 3rd Generation Partnership Project

**5G:** 5th Generation

**AE:** Array Element

**AF:** Array Factor

**AWGN:** Additive White Gaussian Noise

**BF:** Beamforming

**BS:** Base Station

**BW:** Beam-width

**CDMA:** Code Division Multiple Access

**FDMA:** Frequency Division Multiple Access

**FFR:** Fractional Frequency Reuse

**HPBW:** Half-Power Beam-width

**IBI:** Inter-beam Interference

**IoT:** Internet of Things

**LDPC:** Low-Density Parity-Check

**LOS:** Line of Sight

**LTE:** Long Term Evolution

**MAI:** Multiple Access Interference

**MF:** Matched Filter

**MIMO:** Multi-Input Multi-Output

**MLE:** Maximum Likelihood Estimator

**mmWave:** millimeter-wave

**MU-MIMO:** Multi-User Multi-Input Multi-Output

**MUSA:** Multi-User Shared Access

**NOMA:** Non-Orthogonal Multiple Access

**OBF:** Opportunistic Beamforming

**OFDMA:** Orthogonal Frequency Division Multiple Access

**OMA:** Orthogonal Multiple Access

**PDMA:** Pattern Division Multiple Access

**PHY:** Physical

**RAN:** Radio Access Network

**SAC:** Shadow Area Constraint

**SCMA:** Sparse Code Multiple Access

**SIC:** Successive Interference Cancellation

**SNR:** Signal-to-Noise Ratio

**SINR:** Signal to Interference plus Noise Ratio

**SPBS:** Signal Power Based Selector

**SU-MIMO:** Single-User Multi-Input Multi-Output

**TD-WFE:** Time Domain Wiener Filter Estimator

**TDMA:** Time Division Multiple Access

**UE:** User Equipment

# Chapter 1

# Introduction

## 1.1 Background

Non-orthogonal multiple access (NOMA), combined with a power domain key idea, constitutes a promising access technique that can significantly increase the system spectrum efficiency for next generation cellular wireless communication networks [1]. NOMA uses the power domain for multiple access where user equipments (UEs) are served at different power levels. In NOMA, power allocation is an important issue to enhance the achievable rate of each UE due to power-domain multi-user multiplexing [2]. In fact, user demultiplexing is guaranteed through the application of Successive Interference Cancellation (SIC) in the power domain and the allocation of large power differences between paired UEs. Illustration of SIC process is shown and detailed in Figure 1.1 for three mobile UEs where $h_1$, $h_2$ and $h_3$ are UEs' channels gains; $x_1$, $x_2$ and $x_3$ are respective UEs signals; and a set of $N_1$, $N_2$, $N_3$ to denote associated noise values to each mobile UEs' received signal. According to Figure 1.1, three mobile UEs are served by the base station (BS) in downlink by sharing the same frequency portion at different power levels, and different power fractions are provided in a such a way that power allocation is performed according to channel conditions in order to proceed with message signal decoding for each UE. Such large power differences facilitate successful decoding and thus the successful cancellation of the interfering signals [3]. In each transmission, the channel gain is an

important factor, and it helps along the descending decoding process which follows the channel gains order as normalized by noise.

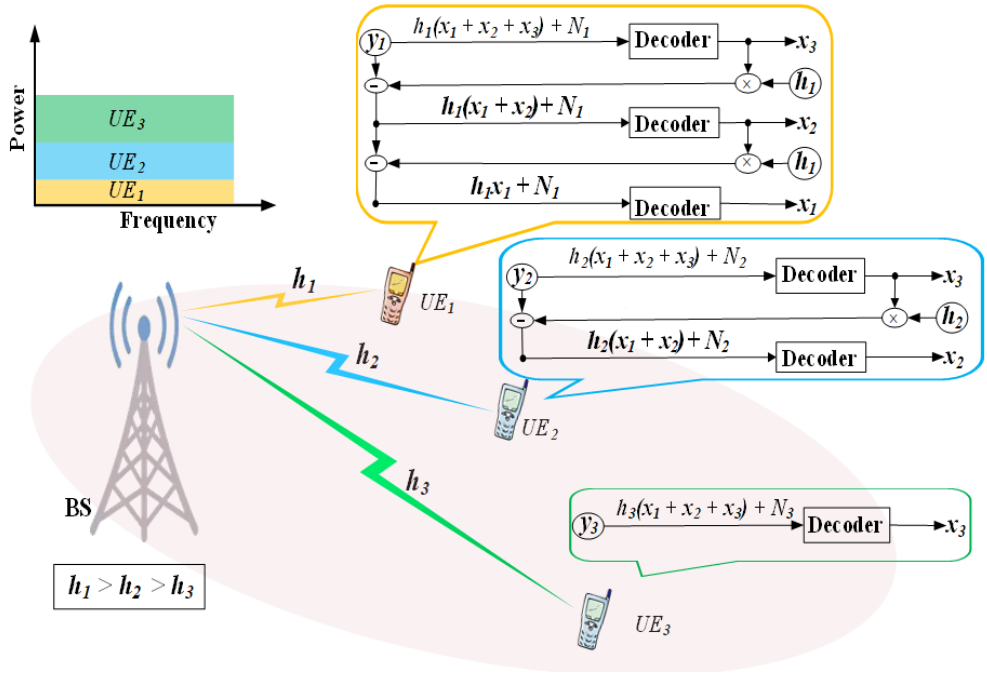


Figure 1.1 NOMA-SIC in Downlink Transmission

In a win-win scenario both UEs, with strong and weak channel gains, may satisfy their needs. The power allocation coefficients, which are the combination coefficients for superposition coding, are determined by UEs' channel conditions. Precisely, a UE with poor channel conditions is allocated more transmission power and a UE's message with a strong channel gain is allocated less transmission power [4]. In fact, intelligent power allocation is critical in wireless networks for improving the spectral efficiency and realizing the users' quality of service (QoS) goals.

The service offered to UE under different channel conditions in a timely manner suggests that it is possible to meet the demanding 5G requirements of ultra-high connectivity and ultra-low latency. It has been clearly shown that NOMA is conceivably compatible with many important 5G technologies, including massive multiple-input multiple-output (massive MIMO), and will be able to sustain more connections than other systems when the massive projected increase in connectivity and transmission via millimeter wave (mmWave) occurs [5,6]. Its applicability can also be extended to many other wireless networks to ensure the preservation of big data key characteristics, handling the high speed and density of vehicles in urban vehicular ad hoc networks and achieving privacy-preserving big data aggregation with fault tolerance in smart grids [7-9].

Research studies have already revealed that, in cellular downlink systems, both total average and cell-edge UE throughput can be improved by NOMA. For example, in evaluations in terms of throughput in a single cell, it has been shown that NOMA, as compared with orthogonal multiple access systems, can achieve large performance gains: approximately 23% for cell average throughput and 33% for cell-edge UE throughput [10-13]. Furthermore, concerning the developed software-defined radio-based NOMA system, the results of a series of over-the-air experiments conducted in indoor experimental scenarios revealed that a NOMA system realizes more than an 18.6% gain in system throughput and more than 84.4% gain in cell-edge UE throughput as compared with an OMA system [14].

To achieve NOMA implementation in the forthcoming generation of cellular networks, there have been various standardization activities. The third-generation partnership project

(3GPP), as a standardization organization, has in particular introduced a study item on downlink multiuser superposition transmission for long term evolution (LTE) in Release 13. It focuses on advanced receiver designs, multiuser non-orthogonal transmission schemes, and other related signaling schemes. Discussions on the further development of LTE in order to meet requirements and identify and provide new solutions to future challenges have been presented [15-17].

Ongoing research on the use of NOMA is being conducted because of scenarios that present a vastly increased need for high-volume services, such as cloud-based services providing image transferal and video streaming, with an improved operation to further enhance system throughput and low latency. Various limitations, such as the decoding complexity on the receiver side and energy consumption, the need to lower the number of UEs within a cluster to reduce the effect of error propagation, restricting the number of user pairs, and NOMA's sensitivity to the uncertainty in the measurement of channel gain information, exist. Thus, implementation issues need to be addressed in order to exploit the advantages of NOMA to the full [18,19].

Research studies are still being conducted in order to solve the limitations to NOMA's implementation. For example, the use of appropriate beamforming (BF) schemes improves the throughput by tripling the system throughput of an E-band point-to-point system, as demonstrated in [20]. The use of BF has also been established for purposes such as improving the system spectrum efficiency by enhancing a desired signal that can be corrupted by interference with the intended UEs from its measurements. The overall system

capacity can then be greatly enhanced within existing resources and actualized in two- and three-dimensions (2D and 3D), depending on the scenarios of the UEs to be served.

However, a high possibility of inter-beam interference (IBI) occurring still remains, for example, in the case of high density UE-scenarios, because of the use of close frequency bands during transmission. The formulation and utilization of BF techniques can contribute to eliminating the interference caused by a high density of UEs within a cluster, in order to reduce data traffic error propagation.

Numerous researches have demonstrated the usefulness of power domain NOMA in 5G cellular networks [21,22]. NOMA as a promising technology can address some of the challenges for 5G such as high spectral efficiency and massive connectivity [23]. The key idea of the proposed scheme in NOMA is to serve multiple users by insuring the cancellation of BF interference. 5G scenario requirements are exemplified in terms of dealing with high user density, providing very high data-rates without delays, super real-time and reliable connections with high levels of service experience. With spectrum handling, the proposed scheme improves the system spectrum efficiency through distinctive beam generation for paired UEs.

## 1.2 Motivation

Many published research articles as well as ongoing projects have focused on beamforming (BF) for different applications in wireless communication field. Some of the research topics such as investigating power allocation among beams in non-orthogonal access with random beamforming, non-orthogonal multiple access (NOMA) in a downlink multiuser BF system, and evaluation of NOMA performance in combination with

opportunistic BF have been carried out to exemplify the use of BF techniques to improve communication capabilities. However, several resolutions have been established in 2-dimension (2D) while practically many mobile user equipments (UEs) are situated in 3-dimension (3D). This thesis considers inter-beam interference cancellation by 3D polarized BF in power domain NOMA systems.

## 1.3 Organization of Thesis

The organization of this thesis is as follows.

Chapter 2 focuses on signal reception for successive interference cancellation in power domain NOMA by a novel NOMA-SIC scheme. The proposed scheme comprises a matched filter, a MF detector and a regenerator at each SIC level. The performance of the proposed novel NOMA-SIC scheme is evaluated in comparison with other SIC-based techniques and demonstrates the best performance on power saving as well as proving the capability of dynamically selecting estimator at each SIC detection level.

Chapter 3 provides the related work on NOMA with beamforming technologies accomplished in different research works. In this chapter, we give an overview on security constraint on the number of user equipments served per beam which is further detailed in Section 5.2.

Chapter 4 gives discussions on NOMA transmission for both uplink and downlink, in the background. NOMA application in OFDM system and 3D multi user-MIMO transmission scenario in NOMA downlink are as well detailed and demonstrated in this chapter.

Chapter 5 develops the inter-beam interference cancellation in power domain NOMA system by 3D polarized beamforming. Beam-width determination, security constraint on the number of user equipments served per beam and power saving for forthcoming network scenario are detailed in this chapter. Chapter 6 gives the performance verification of the proposed IBI cancellation scheme by simulation and the thesis conclusions are drawn in Chapter 7.

# Chapter 2

# Signal Reception for Successive Interference Cancellation in Power Domain NOMA

## 2.1 Introduction

Power saving for wireless system of Internet of Thongs (IoT)-enable devices is one of the biggest challenges with the rapidly growing data traffic demand. Energy efficiency, pivotal as spectrum efficiency, become more critical issue in the design of the network protocols and structures [24,25].

In this chapter, we focus on the design of successive interference cancelation (SIC) in power domain NOMA systems [26-28]. The principle of SIC is to gradually eliminate the maximum signal power of the device's multiple access interference (MAI). Owing to the stronger device's signal power is easier to be captured, the SIC detector will sort the received signals in accordance with the level of received devices' signal power for demodulation. Once demodulating a device signal, then eliminating its MAI, repeat the same operation until the elimination of all MAI. The SIC detects only one device signal during each stage, i.e., SIC level, thus $K$ devices correspond to $K$-level detections. The demodulation outputs of each detection stage include the received signal of the maximum power device and received signal after MAI removal from that device.

## 2.2 Related Works on Successive Interference Cancellation

Various research works have been carried out for the sake of interference cancellation and computational complexity reduction. A low-complexity multiple feedback SIC strategy has been proposed in [29] for multi-device MIMO systems. In the proposed multi feedback SIC with shadow area constraints algorithm, an enhanced multiple device interference cancellation is achieved by introducing the feedback diversity to combat the error propagation in decision feedback loops. The combination of multiple feedback SIC with multi-branch processing demonstrated to achieve a higher detection diversity. For coded systems, a low-complexity soft-input soft-output iterative (turbo) detector is proposed based on the multiple feedback interference suppression and the soft canceler followed by a minimum mean square error scheme.

New detection methods have been investigated in [30] for low data-rate machine type communication where a particular attention is to be considered in uplink communication networks where devices can only be active occasionally. When devices occasionally participate in network, this requires a joint activity and data detection at the receiver side. Research demonstrates that a modified version of successive interference cancellation is a practical method for the detection of low data-rate multi-device signals. The analysis of the proposal considered hardware implementation by particularly investigating algorithmic complexity of the introduced algorithms.

Successful mitigation of error propagation therefore significantly improving the bit error rate performance is a result of an improved multiple feedback successive interference cancellation algorithm proposed in [31]. It is proposed for symbol vector detection in

multiple-input multiple-output (MIMO) spatial multiplexing systems. Based on the concept of shadow area constraint (SAC) where, if the decision falls in the shadow region multiple neighboring, constellation points will be used in the decision feedback loop followed by the conventional SIC. The best candidate symbol from multiple neighboring symbols is selected using the maximum likelihood criteria. However, while deciding the best symbol from multiple neighboring symbols, the shadow area constraint condition may occur in successive layers which results in inaccurate decision. In the proposed algorithm, this limitation is overcome by recursively checking shadow area constraint criteria for each layer. An ordered improved multi feedback successive interference cancellation is also proposed where log likelihood ratio based dynamic ordering of the detection sequence is used and the term dynamic ordering is applied in the sense that the detection order is updated after every successful decision. Comparing results exemplified that the proposed algorithms outperforms existing detectors such as conventional successive interference cancellation and multi feedback successive cancellation in terms of bit error rate and achieves a near minimum likelihood performance.

A set of practical low-density parity-check (LDPC) codes with moderate block size are used to investigate the practical performance of interference cancellation. In order to match the bit error rate performance under the binary phase shift keying modulation, the binary-input channel capacity comparison is used to obtain the theoretical values as benchmark for simulations. In practice, SIC provides a higher transmission rate for the second detected device compared with single-device detection method. The order of signal detection and subtraction also has an impact on the required signal power to achieve the desired

transmission rate. If the previously detected signal is just subtracted, error propagation will occur when the signal was not decoded correctly. For that reason, a “soft” interference cancellation scheme is used to take into account the reliabilities with which bit decisions after channel decoding can be taken [32].

Successive interference cancellation has been widely adopted in the 3rd generation mobile communication systems, i.e., code division multiple access (CDMA) systems, as a multi-device detection technology. In CDMA, the SIC process can effectively remove the MAI to achieve proper demodulations through the characteristics of pseudo-random spreading codes. However, in NOMA systems, the transmitter uses power multiplexing for different devices through power domain distribution, the SIC process needs to be upgraded according to the device’s signal transmission power that to distinguish devices and sort signals for demodulation.

The use of signal transmission power instead of pseudo-random spread codes to distinguish devices is a major difference between 5G and 3G systems for SIC algorithms, thus we cannot simply employ CDMA-based SIC algorithms into 5G systems.

The complexity of *K*-level SIC process for power rearrangement and signal demodulation processes is mainly determined by the number of devices. To improve the NOMA utility, we hope to reduce the NOMA-SIC process complexity by optimizing the system modules such as channel estimation at mobile terminal side. Moreover, the optimization strategies should meet NOMA mechanisms, of which can play its power domain exploration characteristics well. The other contribution of this thesis part thus is the proposed NOMA-SIC scheme, of which the goal is to reduce the computation

complexity, i.e., saving power consumption at demodulation process, guaranteeing the power efficiency, while maintaining the spectrum efficiency.

## 2.3 Computational Complexity for Channel Estimators

Generally, in multi-carrier communication systems, wildly employed channel estimation methods are one-dimensional least square estimator (1-D LSE), maximum likelihood estimator (MLE), Wiener Filter detectors, including 2-D Wiener filter estimator (2-D WFE), 2-by-1-dimensional Wiener filter estimator (2*1 WFE), time domain Wiener filter estimator (TD-WFE) and so on [33-35]. The performance of each channel estimator is related to its computational complexity. Usually, relatively complex detectors have better performances to minimize estimation error. Because NOMA-SIC needs to estimate the channel information of each device, it is possible to flexibly select different channel estimator based on the transmission power of devices at each SIC detection level. This is an effective way to achieve correct estimation with both power and spectrum efficiency concerns, balancing trade-off between complexity and system performances.

Table 2.1 lists the computational complexity for above channel estimators along with the complexity for 3GPP LTE downlinks, where $L$, $N_p$, and $N_s$ are the channel response length, the number of training sequences, and the number of subcarriers, respectively.

By using a fixed bandwidth, we can let $N_b$ denoting the number of physical resource blocks of LTE system to represent the complexity as listed in Table 2.1 as well. From Table 2.1, we find that the computational complexity of estimators is increased from the top to end, where the simulations for error reduction during the estimation processes in literatures

have proved the truth that generally a more complex estimator holds a better performance on error reduction [35].

**Table 2.1 Computational complexity for channel estimators**

| Estimators | Complex Multiplications per Slot | |
|---|---|---|
| 1-D LSE | $9N_s$ | $108N_b$ |
| MLE | $4L\left[\frac{N_p}{2}(L+1)+N_s+\frac{L^2}{2}\right]+7N_s$ | $14436N_b+118638$ |
| MLE + TD-WFE | $4L\left[\frac{N_p}{2}(L+1)+N_s+\frac{L^2}{2}\right]+68N_s$ | $15168N_b+118638$ |
| TD-WFE + MLE | $7L\left[L^2+2LN_p+(2N_p+N_s)\right]+23N_p$ | $90728N_b+415233$ |
| 2*1 WFE | $N_p\left[\left(\frac{N_p}{2}\right)^2+(N_s+1)\frac{N_p}{2}+2N_s\right]+68N_s$ | $16N_b^3+200N_b^2+816N_b$ |
| 2-D WFE | $N_p\left[N_p^2+3N_p+(28+N_p)N_s\right]$ | $256N_b^3+1392N_b^2$ |

## 2.4 System Model

Consider the illustration of Figure 2.1 for the proposed new structure of NOMA-SIC in order to balance the trade-off between complexity and system performance. In Figure 2.1, each NOMA-SIC level is comprised by a matched filter (MF), a MF detector and a regenerator. The MF at each detection process provides a source for regenerating the received device signal by appropriately determining the signal delay, amplitude and phase. The detected signals are re-modulated and performed as the input of regenerator, and subtracted to reconstruct receiving signal for interference cancellation from the original received signal, therewith prepared for further iterations.

A detailed description of the SIC function for 5G systems can be found in [36], whereas the major difference from conventional SIC methods is that we employ the signal power based selector (SPBS) at each SIC detection level. The function of SPBS is to flexibly select estimators during the channel estimation process according to the device transmitting power at each SIC level.

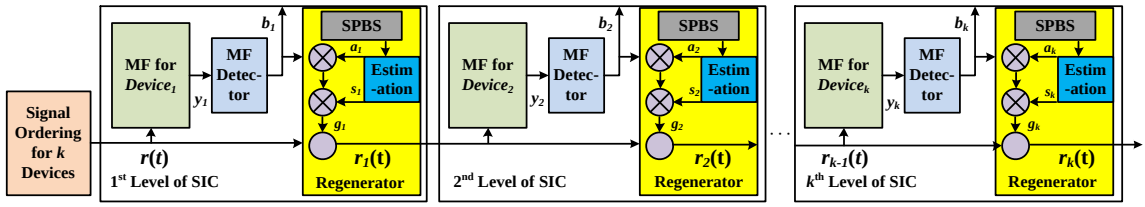


Figure 2.1 The proposed NOMA-SIC diagram.

That is, for the device located near to the base station, it can use low complex estimator to estimate channel information of interfered signal owing to the interfered signal from cell-edge devices is with higher transmitted power. In next SIC level, SPBS can select a more complicated estimator for interference cancellation of closer devices; and finally selects the most complex estimator to cover its own signal. For cell-edge devices, even if it is allocated with the highest transmission power by base station, the SPBS can dynamically select a comparative complex estimator for channel estimation in its solely SIC level for a correct demodulation.

## 2.5 Performance Evaluation of the Proposed NOMA-SIC

In this subsection, Monte Carlo simulations are used to demonstrate energy efficiency metrics. Note that, we employ the transmitting power model of [25] for simulations, where

the deviation parameter of log-normal shadowing is fixed as 8 dB; path-loss exponent over fading channels is two by considering short distance transmissions; and the number of obstacles between transceivers are two. For computing power model, we simplify it by considering a linear relation with estimator computational complexity.

In NOMA system, the mobile devices are grouped into device pairs, where in each pair, the devices communicate with base station in a polling transmission manner. Figure 2.2 then gives the simulation results of energy efficiency of the proposed NOMA-SIC compared with conventional SIC schemes. The proposed NOMA-SIC shows the best performance on power saving, of which the energy efficiency increases with an increase in the number of NOMA device pairs. 2-D WFE-based SIC slightly outperforms 2*1 WFE-based SIC in terms of estimation error reduction [35], however the former one (i.e., 2-D WFE-based SIC) hold higher computational complexity that yields a worse performance on energy efficiency than the latter one (i.e., 2*1 WFE-based SIC) as illustrated by Figure 2.2. On the contrary, although MLE-based SIC holds the lowest computation complexity, compared with others, it does not perform well in estimation error reduction that requires to be assigned a higher transmission power to increase the signal to interference plus noise ratio (SINR) to achieve correct demodulations. Therefore, MLE-based SIC costs the highest power compared with other SICs. The simulation results again prove that the proposed NOMA-SIC can dynamically select estimator at each SIC detection level, guaranteeing the power efficiency and maintaining the spectrum efficiency.

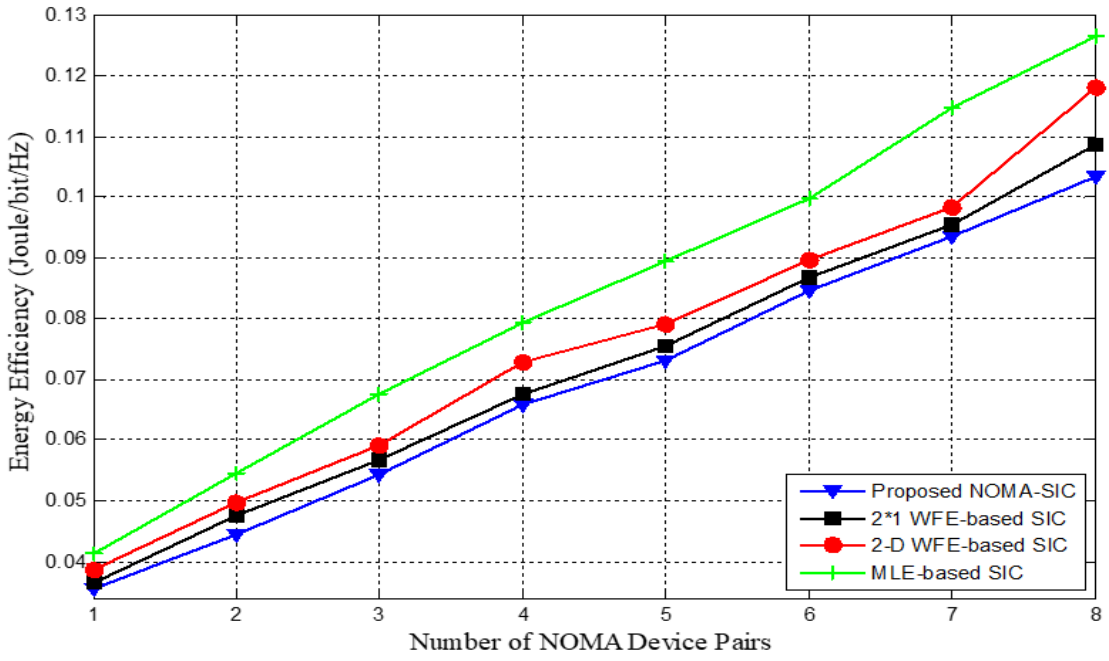


Figure 2.2 Energy efficiency with respect to the number of NOMA device pairs.

## 2.6 Conclusions

In this section, a novel NOMA-SIC scheme is proposed and its performance is evaluated in comparison with other SIC-based techniques and channel estimation methods for example maximum likelihood estimator (MLE), Wiener filter estimators (WFE). Wiener filter detectors include 2-D Wiener filter estimator (2-D WFE), 2-by-1 dimensional Wiener filter estimator (2*1 WFE), time domain Wiener filter estimator (TD-WFE). The proposed scheme comprising a matched filter, a MF detector and a regenerator at each SIC level, outperforms the above mentioned SIC-based techniques. The proposed scheme demonstrates the best performance on power saving, of which the energy efficiency increases with an increase in the number of NOMA device pairs. The novel scheme also

proves the capability of dynamically selecting estimator at each SIC detection level, ensuring the power saving and sustaining the spectrum efficiency.

# Chapter 3

# Related Work on NOMA with Beamforming Technologies

Myriad studies have been conducted on the application of BF techniques in NOMA systems for performance improvement. As a single BF vector is shared by either two or multiple UEs, the spectrum efficiency is prone to be degraded by interference from other BF vectors. A NOMA-based multiuser BF (NOMA-BF) system was proposed in [37].

Power allocation algorithms and clustering are additional techniques to guarantee spectrum efficiency and reduce interference in a NOMA-BF system. The mainstream power allocation algorithms attempt to ensure that transmitting power is allocated to each UE for spectrum efficiency maximization. Since a BF vector simultaneously serves several selected users in a cluster, its total transmit power should be divided effectively among those users. The power division concept causes a change in the UEs' capacities according to the results of exploring the power domain. Therefore, spectrum efficiency is maximized such that equality of the capacity of a weak UE is conserved in NOMA-BF and in conventional multiuser BF systems. It is desirable to keep the weak UE capacity greater in NOMA-BF than in a conventional multiuser BF system.

A clustering algorithm is implemented to mitigate interference from other beams by applying a two UE selection. This is achieved by considering the high correlation and large gain-difference between the channels of the selected users in a cluster, as in the scenario depicted in Figure 3.1, where two UEs in one beam are given as an example. If the channels

of the strong and weak UEs (i.e., the UEs having a larger or smaller channel gain, respectively) are highly correlated, the inter-cluster interference of the weak UE can progressively be reduced. $UE_{1,1}$ is the first UE in the first cluster with $h_{1,1}$ channel gain through beam $BF_1$. In the same form, $h_{2,1}$ denotes the channel gain of, $UE_{2,1}$, the second UE in the first cluster served by beam $BF_1$, respectively. Similarly, $UE_{1,N}$ denotes the first UE of the $N^{th}$ cluster with $h_{1,N}$ channel gain through beam $BF_N$ and $h_{2,N}$ denotes the channel gain of, $UE_{2,N}$, the second UE of the respective $N^{th}$ cluster served by beam $BF_N$, respectively.

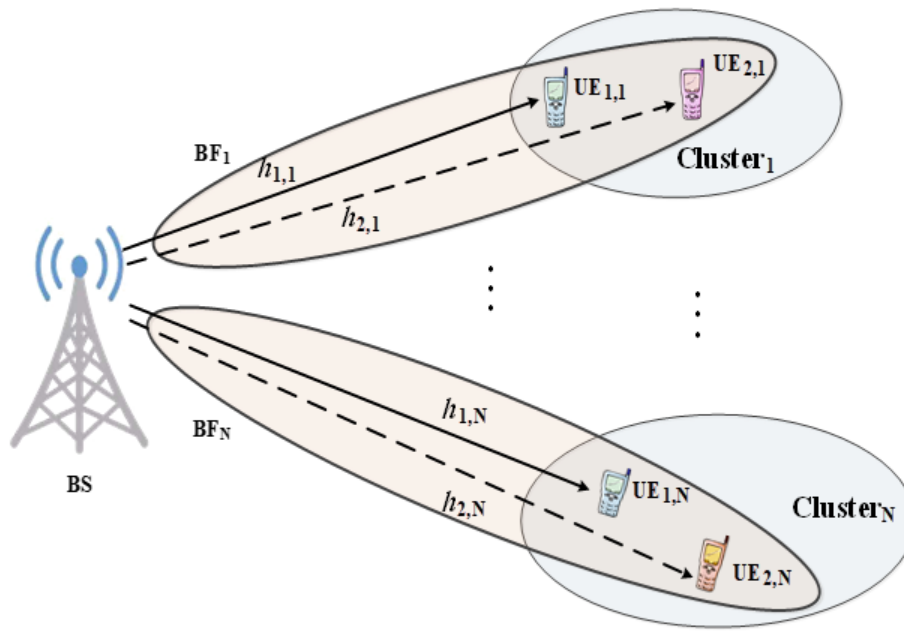


Figure 3.1 Use of beamforming for NOMA users grouped in clusters.

The power difference between the messages received by the two UEs becomes large under the condition that the channel gain-difference between the two UEs is significant.

The allocation leads to unequal power distribution, with high power allocation to the weak UE and low power allocation to the strong UE, guaranteed by the general downlink successive interference cancellation (SIC) technique. In addition, when the weak UE experiences inter-user interference, this inter-user interference will be reduced provided that the strong user's signal power decreases.

Because NOMA-BF has been proven to enhance the system sum capacity, NOMA combined with opportunistic BF (OBF) has also been suggested as a useful multi-antenna transmission scheme [38]. In this combination, random beams are created by using OBF in the spatial domain and NOMA is applied in each beam to exploit the power domain and efficiently use the spatial domain. That is, the transmit-receive process in NOMA with OBF is assured such that the base station (BS) sends the reference signal and performs UE scheduling and data transmission. Meanwhile, the user performs channel measurement and feedback and data reception. In the enhanced form of OBF, the BS commits to memory the precoding matrices that achieve a significant user throughput, and returns to memory for scheduling, together with selection of the best precoding matrix and corresponding users for data transmission. A large performance gain is then achieved by NOMA with OBF.

The authors of [39] presented a non-orthogonal access scheme with random BF and intra-beam SIC for cellular MIMO downlink to further improve the cell-edge user experience and the efficiency of the system. The proposed scheme for obtaining a better overall sum rate and cell-edge user throughput is described in detail. The use of superposition coding and SIC for non-orthogonally multiplex multiple users within a beam is considered in particular. The spatial filtering serves to suppress the IBI at the user

terminal only by using multiple receiver antennas. The intra-beam SIC mitigates the inter-user interference produced by intra-beam superposition coding within a beam. For the interference cancellation process, the decoding order reaches its optimality when increasing the normalized channel gain. Throughout the random BF process [39,40], before transmitting the real data, the BS arbitrarily defines the BF vectors without the aid of any feedback information from the user terminals, and then, sends the downlink reference signals beam formed by the predefined BF vectors. Depending on the reported signal to interference plus noise ratio (SINR), the user scheduling is executed for each beam and transmission of data.

The determination of the BF matrix can be featured by the random BF application. For limited channel state information feedback reduction, random BF has been identified as an effective method to effectively achieve a significant spatial multiplexing gain, together with multiuser diversity, when the resource is appropriately and strategically allocated. Hayashi et al. reported in [40] their investigation of power allocation among beams in the non-orthogonal access case, where the power distribution is examined with random BF and intra-beam SIC for cellular MIMO downlink. The proposed joint transmission power allocation control method, which concerns different frequency blocks and beams, improves the trade-off between the cell-edge and the average user throughput. The design is based on the fractional frequency reuse (FFR) principle and frequency block-dependent power allocation among multiple beams. Because of the difference in the transmission power of the frequency block at the inner band (with reduced transmission power) and edge bands (with increased transmission power), a better SINR at the edge band is achieved by inter-

cell interference coordination. FFR achieves a tradeoff between the effect of inter-cell interference mitigation and the utilization efficiency of the frequency bandwidth per cell. Simulation results show that the average user throughput is decreased while cell-edge user throughput is increased. These results were obtained for an increased transmission power dissimilarity, where a different power allocation parameter was considered. The great increase and slight decrease in cell-edge and in-cell average user throughputs, respectively, is achieved by coordinating the inter-beam and inter-frequency block power allocations.

According to the survey of related work, there remain open problems and challenging research tasks to accomplish to further improve NOMA systems' capability. The BF method is one of the most efficient methods for increasing NOMA performance in terms of user throughput, fairness, interference cancellation, and so on.

Most of the conventional work focused only on 2D BF methods for NOMA systems. However, in reality, UEs are distributed in a space and need to be efficiently served. The extension to 3D BF is necessary to bring NOMA systems closer to practicability in everyday use, e.g., in 5G. The details of the proposed 3D BF-based NOMA system are described in the remaining sections of this thesis.

To meet the demanding challenges of 5G networks, innovative technologies on radio air-interface and radio access network (RAN) are of great importance in PHY designs. Besides several radio access technologies such multiuser shared access (MUSA), sparse code multiple access (SCMA) and pattern division multiple access (PDMA), NOMA has recently attracted increasing research interests from both industrial and academic fields as a powerful radio access technique [41].

Despite distinctive features which make NOMA to stay as the strongest candidate for future 5G networks, there are still some challenges for its successful implementation. Practically, NOMA implementation in cellular networks requires high computational power to implement real-time power allocation and run SIC algorithms particularly for high number of UEs at high data rates. When UEs are particularly moving fast in network, power allocation optimization remains as a challenging problem, and also the sensitivity of the SIC receiver to cancellation errors can easily occur in fading channels. Within targeted time, that is by 2020, for the deployment of 5G networks, the computational capacity of both handsets and access points is expected to be high enough to run NOMA algorithms [42].

Implementation of NOMA with massive MIMO as discussed in [5,6] or with coding schemes can accordingly reduce the decoding errors and increase the reliability. There are also works that implement MIMO for NOMA [43], [6]; the impact of channel state information and capacity maximization problem are studied in [44], and outage probability expressions are derived in [45]. Digital beamforming which can offer the most versatile solution for future 5G communication systems can point a signal from sender to receiver when they are in line of sight (LOS). In non-LOS scenario, UEs are only reached by scattering resultant signals.

Security is always an important issue in system design because of the broadcasting nature of the wireless channel. Since the PHY layer is the lowest in the protocol stack, which determines the most basic functions, the PHY layer security has received more attention [46,47]. In general, two primary attacks threaten physical security: jamming and

eavesdropping. Jamming is a scheme that attacks the transmitter, e.g., by occupying the channel, and handicaps its correct operation, whereas an eavesdropping attack is an attack at the receiver side that collects a transmitted signal and attempts to interpret the contents. The eavesdropping attack is more difficult to discover, since it almost silently completes its objective.

MIMO and NOMA are two building techniques of 5G that are intensively being studied. In the multiple antenna (MIMO) and NOMA background, where various signals are mixed together, the regulation and security of the physical conditions demand more effort. In a MIMO NOMA system, the broadcasting signal becomes focused by virtue of the BF. However, by the nature of NOMA, the signals of different users are overlapped and superposed, which risks physical security. In [48], a similar case of interference alignment was considered and closed forms are given for secure transmission. The maximization of the secrecy sum rate of a single-input single-output (SISO) NOMA system regarding power allocation was addressed in [49]. More meaningful results are provided in [50] for the single and multiple antenna cases.

The secrecy outage probability was derived for both cases. We address this problem in the 3D-BF setting in Section 5.2.

# Chapter 4

# System Model

## 4.1 Background

We consider the NOMA situation with a given number $N$ of UEs. For uplink, the transmitted signal by $N$ UEs to the BS can be expressed as

$$y(t)=\sum_{i=1}^{N} x_i(t)+n_i(t), \tag{4.1}$$

where $x_i(t)$ is the encoded UE$_i$'s signal with $i$=(1,2, ...,$N$) to satisfy $E\left[x_i^2(t)\right]\le P_i$; this power constraint is such that all users occupy the same bandwidth $W$. $n_i(t)$ is the additive white Gaussian noise with power spectral density $N_0/2$. The channel access capacity is then given by

$$\sum_i R_i \le W\mathrm{lb}\left(1+\frac{\sum_i P_i}{N_0 W}\right). \tag{4.2}$$

Assume that two UEs are transmitting on an uplink multiple access channel based on (4.2). At the receiver, the SIC is required for the encoded signals in order to achieve the situation depicted in Figure 4.1 for the capacity bounds, as power fractions are unequally allocated to UEs according to channel conditions. Points E and F represent the $UE_1$ and $UE_2$ channel capacity holding for all resources, respectively. The SIC-based approach cannot directly reach the capacity of the line segment L—K.

For given 2 UEs capacity bounds as illustrated in Figure 4.1, the process to obtain the illustrated situation can be achieved through applying different techniques such as successive interference cancellation, time sharing or rate splitting. The success of SIC depends on the perfect cancellation of signals in iteration steps. The transmitter should accurately split power between the user information waveforms and superimpose them. In association with time sharing or rate splitting, the capacity of line segment L—K can be achieved. The capacity represented by curve F—P—E can here be achieved by using frequency division multiple access, and to achieve the capacity of dotted line F—E, time division multiple access is considered.

For the time division multiple access (TDMA) in (3) and frequency division multiple access (FDMA) in (4) transmission cases, we assume two UEs occupying $T_1$ and $T_2$ for duration $T$ and $W_1$ and $W_2$ in bandwidth $W$, respectively, with power constraints satisfaction. Their respective channel capacities are represented by the dotted line in Figure 4.1 and expressed as

$$R_1 = \frac{T_1}{T} W \mathrm{lb}\left(1 + \frac{P_1}{N_0 W}\right), R_2 = \frac{T_2}{T} W \mathrm{lb}\left(1 + \frac{P_2}{N_0 W}\right) \tag{4.3}$$

and

$$R_1 = W_1 \mathrm{lb}\left(1 + \frac{P_1}{N_0 W}\right), \; R_2 = W_2 \mathrm{lb}\left(1 + \frac{P_2}{N_0 W}\right) \tag{4.4}$$

We further improve the capacity of (3) and (4). With the power constrains of $T^{-1}\int_0^T E\left[x_i^2(t)\right] \le P_i$ in time duration $T_i$ for UE$_i$, the power can be increased to $E\left[x_i^2\right] \le P_i T/T_i$ for TDMA, and allowing UE$_i$ to transmit with the highest power at bandwidth $W_i$ in FDMA, the channel capacities are, respectively, defined by

$$R_1 = \frac{T_1}{T} W \mathrm{lb}\left(1+\frac{P_1 T}{T_1 N_0 W}\right),\ R_2 = \frac{T_2}{T} W \mathrm{lb}\left(1+\frac{P_2 T}{T_2 N_0 W}\right), \tag{4.5}$$

and

$$R_1 = W_1 \mathrm{lb}\left(1+\frac{P_1}{N_0 W_1}\right),\ R_2 = W_2 \mathrm{lb}\left(1+\frac{P_2}{N_0 W_2}\right). \tag{4.6}$$

The TDMA and FDMA capacities can then reach point **P,** as shown in Figure 4.1; however, $R_1 << R_2$ at point **P** in the event that fairness amongst users is poor [51] occurred when the transmission powers of the UEs were unequal.

For downlink, the BS transmits a superposed signal to $N$ users with a fraction $\varphi_i$ of the total power to UE$_i$ such that $P_i = \varphi_i P$, where $P$ is the total power. The UE$_i$'s received signal is denoted by

$$y_i(t) = h_i s(t) + n_i(t), \tag{4.7}$$

where $s(t)$ is given by

$$s(t) = \sum_{i=1}^{N} \sqrt{\varphi_i P}\, x_i(t), \tag{4.8}$$

where $h_i$ is the complex channel coefficient, $s$ is the BS transmitted signal, and $x_i$ is the signal for UE$_i$. For a perfect superposition coding at the BS and SIC at UE$_i$, the achievable data rate for UE$_i$ is

$$R_i = W\text{lb}\left(1+\frac{\varphi_i P|h_i|^2}{P|h_i|^2\sum_{k=1,k\neq i}^{N}\varphi_k + N_0}\right). \tag{4.9}$$

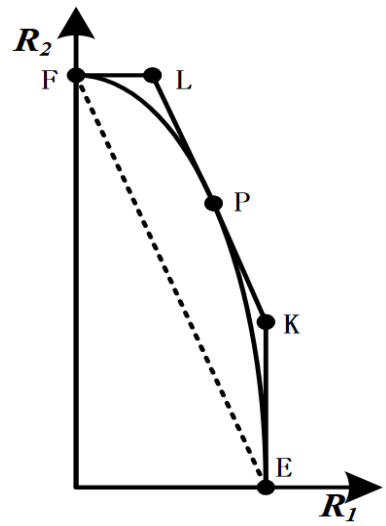


Figure 4.1 Two user equipment's multiple-access channel capacity bounds with unequal power

## 4.2 NOMA Applied in OFDM System

Orthogonal access, such as orthogonal frequency division multiplexing (OFDM), with a simplified receiver design, is also a practical choice for reaching a significant system

throughput. NOMA schemes can be integrated into OFDM systems, as shown in Figure 4.2, for multiple UE transmissions. The goal of this integration is to enhance the system throughput, as well as to provide backward compatibility for LTE multi-carrier systems. Such systems show an ability to achieve a robust gain provision performance, irrespective of the user mobility or feedback/processing latency in practical wide area deployments [52]. As illustrated in Figure 4.2, the power domain multiplexing is implemented between the system block of the inverse fast Fourier transform (IFFT) and the system block of parallel to serial (P/S) converter at the transmitter; accordingly, the NOMA SIC is performed between the system blocks of FFT and S/P at each UE.

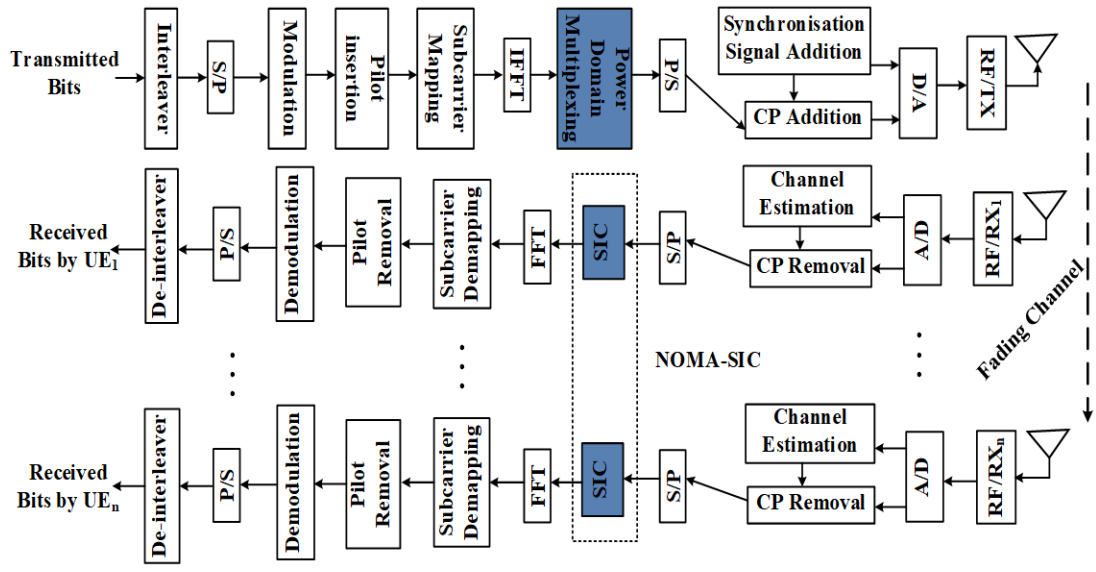


Figure 4.2 Applying NOMA technology in OFDM system.

## 4.3 Three-dimensional Multiuser Multiple-input Multiple-output Transmission Scenario in NOMA Downlink

For the downlink channel, *N* UEs' received signals can be expressed as

$$\mathbf{y}_N = \mathbf{H}_{\mathrm{DL}}\mathbf{s}_N + \mathbf{n}_N, \tag{4.10}$$

where $\mathbf{H}_{\mathrm{DL}}$ represents the channel matrix between the BS and UEs, **s** is the transmit signal vector from the BS, and **n** denotes the noise vector. In multi-user MIMO (MU-MIMO) systems, the BF technology can offer numerous gains exemplified in the increase in the SINR and support of higher user densities. Using an active antenna array at the BS can lead to adaptive UE specific 3D-BF in both the vertical and horizontal direction, as demonstrated in Figure 4.3.

Figure 4.3 illustrates a transmission scenario where a bundle of beams is sent to different users, distributed in a space, in both the horizontal and vertical domain. In the case of vertical BF, access points (APs) in the vertical plane are used to reliably serve the UEs at different locations on different floors in a skyscraper (tall building). In the horizontal BF, numerous and widely distributed UEs are served in the horizontal plane. In the figure, the IBI occurrence is depicted within beams serving many closely spaced UEs [53].

The spatial Poisson point process according to which, for nodes in a unit area, the probability that there are *N* nodes in *A* is given by the Poisson distribution:

$$P(N) = \frac{(\lambda A)^N}{N!} e^{-\lambda A}, \tag{4.11}$$

where $\lambda$ denotes the node density in a unit area $A$. The Poisson point process can represent the mobile users in a macro-cell; the Poisson cluster process for node clustering with independence between cluster locations can be used to represent femto-cells (hotspots) [54,55]. The performance of a sharp beam in BF interference mitigation is evident. However, it is inefficient to assign all array elements (AEs) of a spatial multiplexer to form one beam, in particular when serving UEs located at the cell edge. This is because AEs can be divided into many different groups in order to form beams for distinct UEs [56].

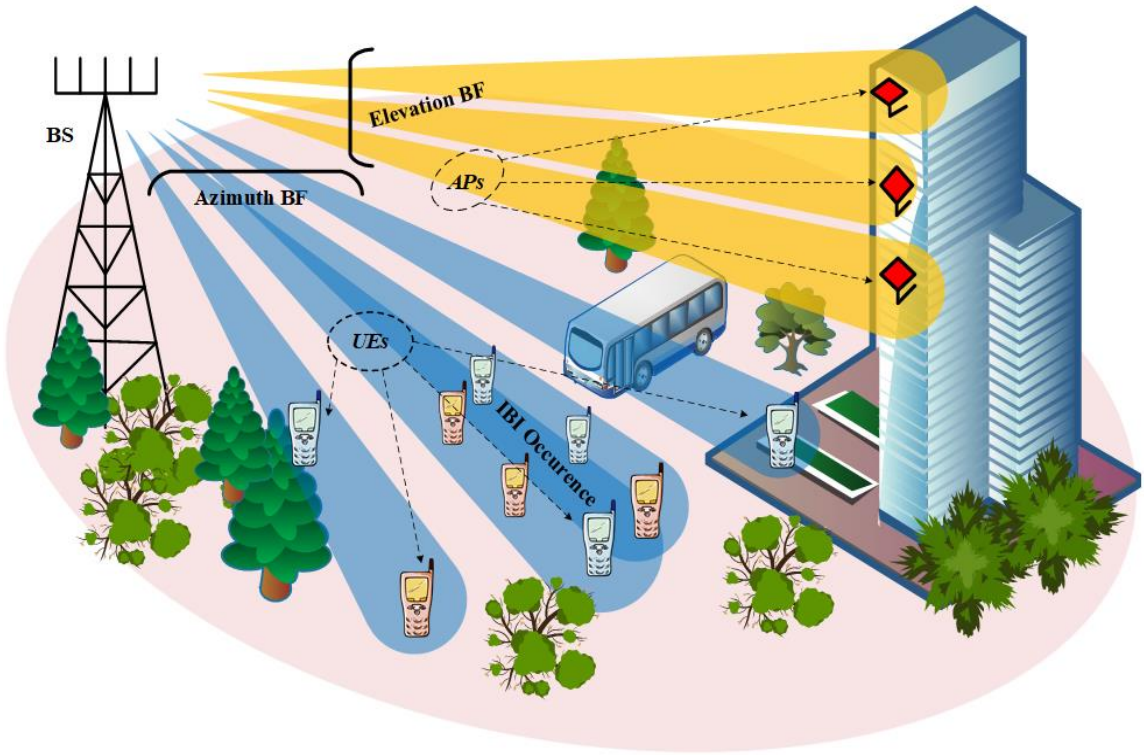


Figure 4.3 Three-dimensional multiuser multiple-input multiple-output transmission scenario in NOMA system.

Consider two beams pointing to two adjacent UEs, in pairs, at the same time. Figure 4.4 shows a situation where $L$ is the beam coverage; $D_3$ and $d_2$ denote the distance from $UE_3$ to the BS and the distance within adjacent UEs (i.e., $UE_3$ and $UE_4$), respectively. The closeness of the UEs can be expressed by approximated equalities $d_1 \approx v_1$ and $d_2 \approx v_2$.

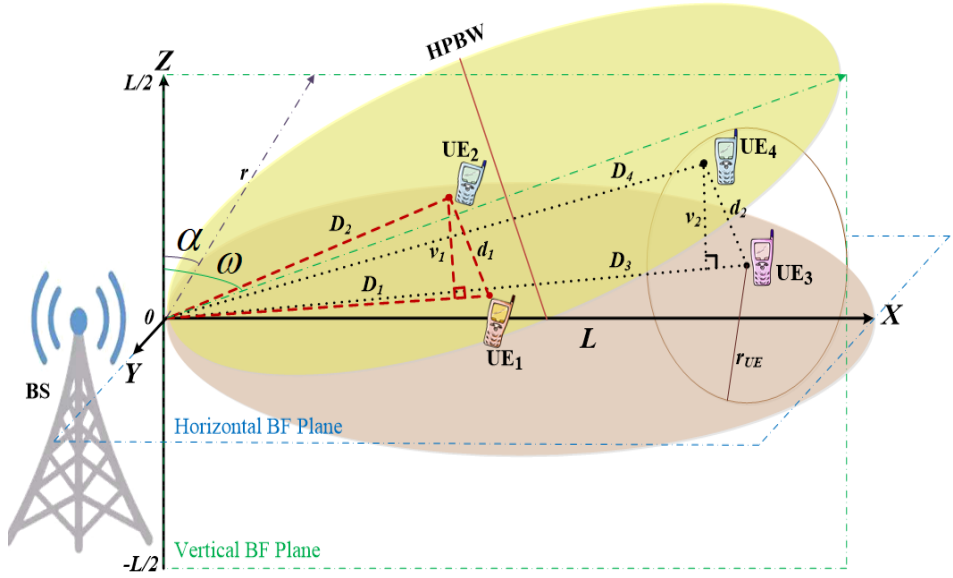


Figure 4.4 Illustration of beam steering to adjacent user equipments and calculating $D_3$ and $d_2$.

For $UE_1$ and $UE_2$ located at 3 dB BW, i.e., in the HPBW area, the BF interference avoidance is assured by controlling the HPBW at less than $2d_1$. In addition, for $UE_3$ and $UE_4$ located in the beam peak area, it is possible to set the HPBW larger than $2d_2$. Assuming UE distribution in a cell and that the situation can be treated as a skyscraper for vertical BF

or a city block for horizontal BF, the average $D_3$ and $d_2$ can be computed. The number of UEs, following the spatial Poisson process with intensity $\lambda$, inside a cell, can be given by

$$K = \lambda L^2. \tag{4.12}$$

The computation of the average distance between the BS and $UE_3$ gives

$$\begin{aligned} D_3 &= \iint_{L^2} \frac{1}{L^2} r dr d\alpha \\ &= \frac{2}{L^2}\left(\int_0^{\omega}\int_0^{a/\cos\alpha} r^2 dr d\alpha + \int_{\omega}^{\pi/2}\int_0^{2a/\sin\alpha} r^2 dr d\alpha\right) \\ &= \frac{\xi L}{2}, \end{aligned} \tag{4.13}$$

where $\xi = \ln(2+\sqrt{5})/12 + \sqrt{5} - 2\ln((\sqrt{5}-1)/2)/3 \approx 1.187$.

The average distance within two adjacent UEs, for example, $UE_3$ and $UE_4$, is given as

$$\begin{aligned} d_2 &= \iint_A \frac{1}{A} r dr d\alpha \\ &= \int_0^{2\pi}\int_0^{r_{UE}} \frac{r^2}{\pi r_{UE}^2} dr d\alpha \\ &= \frac{2}{3} r_{UE} \end{aligned} \tag{4.14}$$

where $A$ is the $UE_3$ local coverage area with radius $r_{UE}$ depending on $\lambda$. As the computed value $D_3$ is close to $L/2$, for BF interferences avoidance, the relation HPBW < $2d_2$ is to be maintained.

The HPBW relation in [57] is given as

$$HPBW \approx 2\left|\arcsin\left(1.391\frac{\varepsilon}{\pi N}+\sin\alpha_0\right)\right| < \frac{4}{3}r_{UE}, \tag{4.15}$$

where $\varepsilon$ is the array spacing factor; that is to say, $\varepsilon = \eta/s$ with $\eta$ and $s$ denoting respectively the signal wavelength and array spacing. $\alpha_0$ represents the incidence angle of the signal shifted from the off-bore-sight direction and $N$ is the number of AEs. An example is that, if $r_{UE} = 15$ meters, at least 8 AEs are needed to overcome BF interferences when $\varepsilon = 2$ and $\alpha_0 = \pi/4$.

The use of a dipole antenna may lead to a decrease in the number of AEs required, because it does not follow the structure of antenna when radiating in longitudinal direction. This can maintain a higher radiation gain than can an isotropic antenna.

# Chapter 5

# Inter-Beam Interference Cancellation in Power Domain NOMA System by Polarized Three-Dimensional Beamforming

In this chapter, we derive the necessary BW in the process of beam pattern generation for IBI cancellation. We also consider the PHY layer security constraints on the number of UEs served per beam and power saving for forthcoming network scenario. Various parameters, such as the number of AEs, AE spacing, and off-boresight angle, are taken into consideration. Array antenna systems are frequently used to enhance the received SINR in a heavily congested operating environment.

## 5.1 Beam-width Determination

The BW is usually understood to mean the HPBW, and both the horizontal and vertical BWs are typically considered in massive MIMO systems. Assuming that most of the radiated power is not divided into side-lobes, the directive gain is inversely proportional to the BW: as the BW decreases, the directive gain increases.

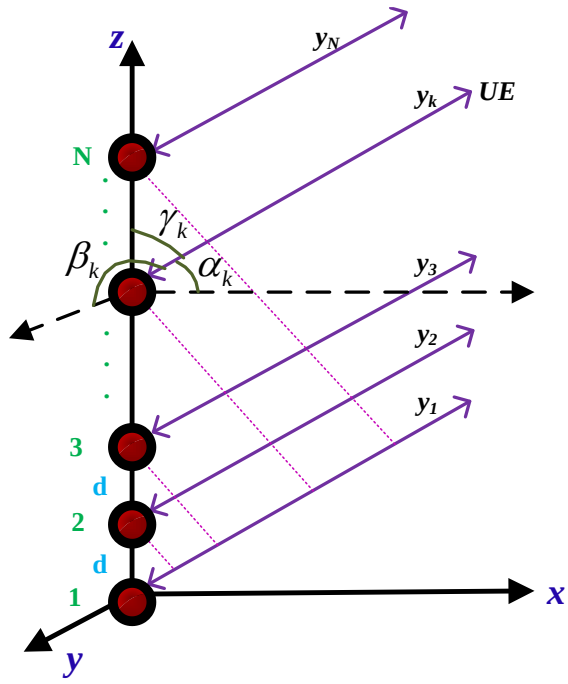


Figure 5.1 Uniform linear array.

Figure 5.1 illustrates a geometric uniform linear array, where equally *d*-spaced elements form a linear array system composed of *N* elements with incident signals $(y_1,...y_{k,}...y_N)$ from system users. We consider acute incidence angles $(\alpha_k,\beta_k,\gamma_k)$ evaluated for their maximum values in the $[0,\pi/2]$ interval according to the *x*, *y*, and *z* directions during the signal reception. An AE branch set for beam generation can be selected for both horizontal and vertical BF through an incident signal of the $k^{th}$ UE, where the maximum value of the acute angle allows the incident signal to be classified with respect to the AE branch selection in the beam generation process [57].

At the same time, IBI becomes highly probable because of the large number of UEs (high user density). The appropriate AE deployment is important in order to concentrate the exact generated beams to specific UEs. By user-pairing, two different UEs can share a beam (same time-frequency resource). In the case where the scenario presents 12 UEs in a 3-sector station (sectoring with 120°/sector), we obtain the situation represented in Figure 5.2.

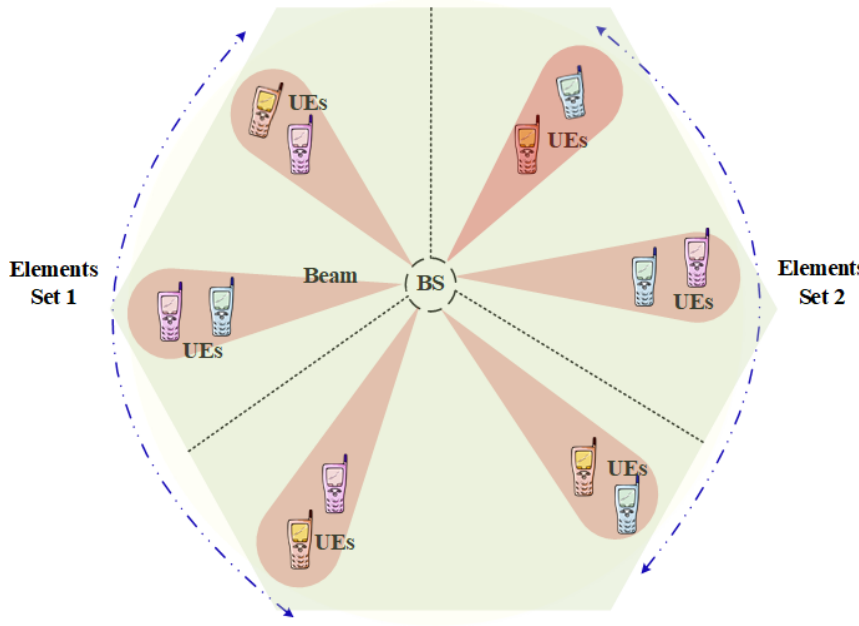


Figure 5.2 Elements sets disposition towards user equipment.

Assuming a perfect polling process and equipartitioned UEs, we can mathematically obtain the required number of AEs to eliminate the IBI. For a complete partition, the spectrum efficiency is given by the number of beams with the number of UEs served by a

beam and the modulation order. For example, one AE with three beams serves three pairs of users, that is, six UEs up to a data rate of 12 bps with quadrature phase shift key (QPSK) and 32 AEs with 96 beams can serve 192 UEs with an achievable spectrum efficiency of 384 bps with QPSK.

In order to determine the required BW, it is essential to consider many key parameters to avoid beam extension and to cancel the IBI, as stated in the process flowchart shown in Figure 5.3. Since we are studying a single cell in a NOMA downlink, the density of UEs in a cell must be carefully considered and analyzed. The assignment of different transmission frequencies in a congested portion of the cell, where the density is high, is advisable in order to avoid interference. For NOMA systems, the proposed IBI cancellation scheme is subdivided into four phases in which different tasks must be performed, as illustrated in Figure 5.3.

The AE selection process in the proposed scheme assigns initial values of the number of AEs, AE spacing, the off-bore-sight angle, and user density in the NOMA cell, as shown in Phase I. In addition to values assignment, the scheme considers different acute angles according to the incident signals. During Phase II, the scheme analyses cell user density and assigns frequencies depending on the congestion situation in a cell. Maximum value for each angle is considered in order to generate an appropriate beam. AEs sequential selection is performed in order to determine and achieve the desirable BW according to the number of engaged AEs.

The maximum value of the acute angle leads to the classification of an incident signal depending on the selected AE branch for sake of suitable operation of UE, as shown in

Phase III. In Phase IV, after classification of the UE's signal, the proposed scheme sets up branches for the specified UE. The gain exploration type that uses polarized 3D beams can maintain the user performances in terms of diversity gain if the incident signal belongs to the cell-edge UEs. Otherwise, spatial multiplexing via polarized 3D beams is proposed to improve the system throughput.

The selection of AEs influences the beam pattern such that the greater the number of elements selected, the more the generated beam is narrowed in 3D-BF, because the HPBW is lowered in degrees according to the increased number of AEs and the AE spacing [57,58]. Table 5.1 presents the HPBW and gain values in terms of varying $\eta$, respectively, where $\eta$ denotes the signal wave-length.

Table 5.1 Half power beam-width and gain for different *N* values and element spacing

| | $\eta/10$ | | $\eta/4$ | | $\eta/2$ | | $3\eta/4$ | |
|---|---|---|---|---|---|---|---|---|
| Elements *N* | HPBW (degrees) | Gain (dB) | HPBW (degrees) | Gain (dB) | HPBW (degrees) | Gain (dB) | HPBW (degrees) | Gain (dB) |
| 2 | 90.83 | 2 | 89.8 | 2 | 83.77 | 2 | 52.57 | 2 |
| 3 | 87.39 | 5 | 70 | 5 | 42 | 5 | 27.64 | 5 |
| 4 | 85.44 | 9 | 62 | 9 | 29.76 | 9 | 19.63 | 9 |
| 10 | 53.37 | 19 | 23.62 | 19 | 10.29 | 19 | 6.8 | 19 |

Note that, the studies presented in [59-61] confirmed that vertical and horizontal sectorizations can increase system throughput in network performance evaluation by considering a dedicated beam pattern design using 3D-BF techniques [62].

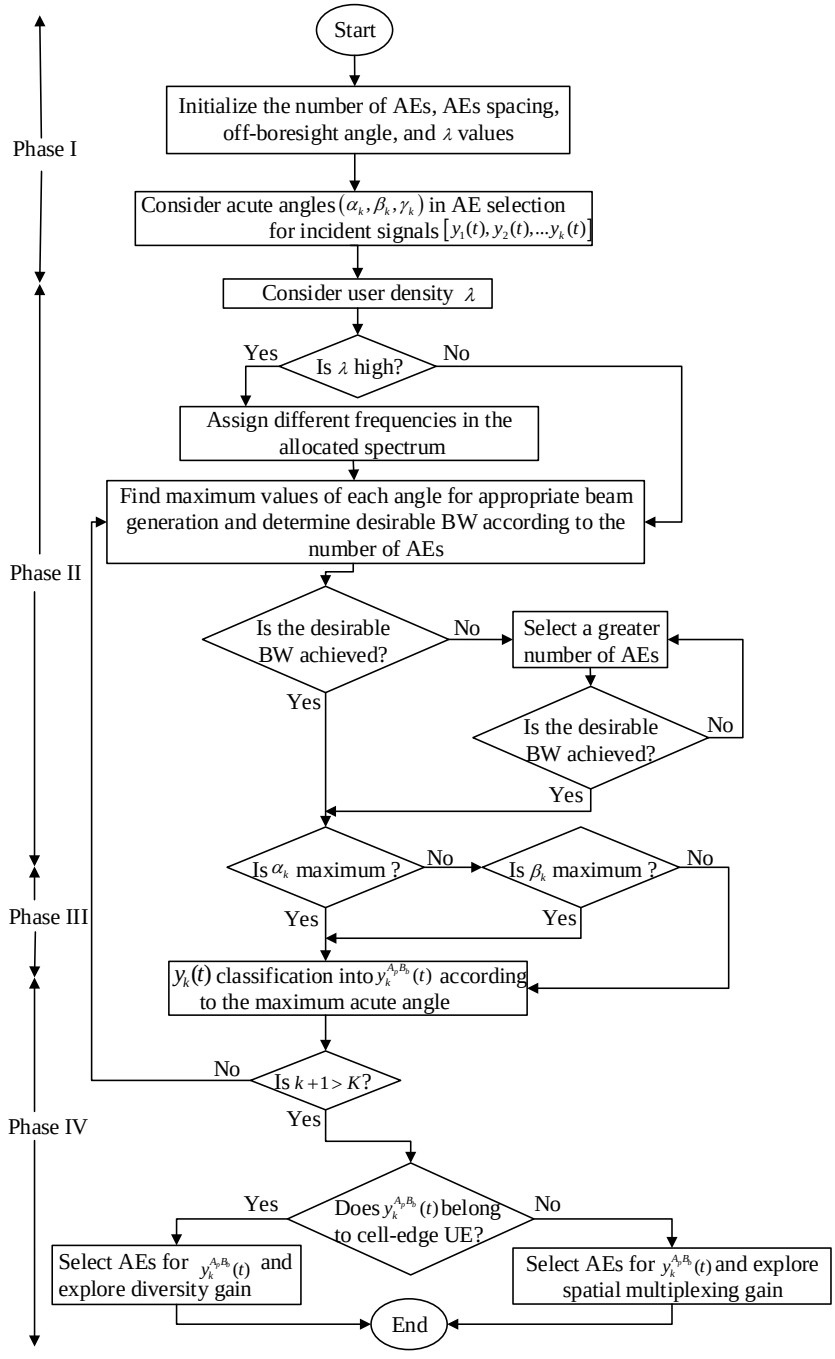


Figure 5.3 Flowchart of the proposed inter-beam interference cancellation for NOMA systems.

The far-field radiation of an isotropic uniform linear array in [63] is represented by an array factor (AF) for an array system. The expression of the AF is in terms of the weighting vector and array propagation vector inner product, and it can finally be computed as

$$AF(\alpha) = \sum_{m=1}^{M} e^{(m-1)(2\pi/\varepsilon)\sin(\alpha-\alpha_0)}, \tag{5.1}$$

where $\varepsilon$ is the array spacing factor with respect to the array configuration, and $\alpha_0$ denotes the specific angle shifted from the boresight direction.

Considering the off-boresight angle, the BW increases when the beam steers to an angle far off the boresight direction. The HPBW is approximated as in (15) with the implication that the BW is inversely proportional to the number of AEs and AE spacing, as specified, but directly proportional to the off-bore-sight angle $\alpha_0$.

The deployment of three dipoles arranged side by side along the z, y, and x-axis allows the triple polarized system 3D radiation pattern to be obtained. The radiation pattern formulations are based on Equation (11) in [57], and the multiplication of the AF quantity and radiation pattern of a single polarized antenna gives the respective polarized uniform linear array beam radiation patterns.

Considering $P_{B_1}(\alpha, \beta, \alpha_{0,1})$, $P_{B_2}(\alpha, \beta, \alpha_{0,2})$, and $P_{B_3}(\alpha, \beta, \alpha_{0,3})$ to be the beam radiation patterns engendered by three dipoles, namely, $A_n B_1$ (the antenna branch 1 of $n^{th}$ array element [57]), $A_n B_2$, and $A_n B_3$,the beam radiation patterns can mathematically be defined by

$$
\begin{aligned}
P_{B_1}\left(\alpha,\beta,\alpha_{0,1}\right) &= \sum_{m=1}^{M} a_{B_1} e^{j(m-1)(2\pi/\varepsilon)\left(\sin\alpha-\sin\alpha_{0,1}\right)} \\
&= a_{B_1}\frac{\sin\left[\left(\pi N/\varepsilon\right)\left(\sin\alpha-\sin\alpha_{0,1}\right)\right]}{N\sin\left[\left(\pi/\varepsilon\right)\left(\sin\alpha-\sin\alpha_{0,1}\right)\right]}, \\
P_{B_2}\left(\alpha,\beta,\alpha_{0,2}\right) &= \sum_{m=1}^{M} a_{B_2} e^{j(m-1)(2\pi/\varepsilon)\left(\sin\beta-\sin\alpha_{0,2}\right)} \\
&= a_{B_2}\frac{\sin\left[\left(\pi N/\varepsilon\right)\left(\sin\beta-\sin\alpha_{0,2}\right)\right]}{N\sin\left[\left(\pi/\varepsilon\right)\left(\sin\beta-\sin\alpha_{0,2}\right)\right]}, \\
P_{B_3}\left(\alpha,\beta,\alpha_{0,3}\right) &= \sum_{m=1}^{M} a_{B_3} e^{j(m-1)(2\pi/\varepsilon)\left(\sin(\frac{\pi}{2}-\beta)-\sin\alpha_{0,3}\right)} \\
&= a_{B_3}\frac{\sin\left[\left(\pi N/\varepsilon\right)\left(\cos\beta-\sin\alpha_{0,3}\right)\right]}{N\sin\left[\left(\pi/\varepsilon\right)\left(\cos\beta-\sin\alpha_{0,3}\right)\right]},
\end{aligned}
\tag{5.2}
$$

where $\alpha_{0,1}$, $\alpha_{0,2}$, and $\alpha_{0,3}$ are the off-boresight angles respectively to $A_nB_1$, $A_nB_2$, and $A_nB_3$.

## 5.2 Security Constraint on the Number of User Equipment served per Beam

The number of UEs served per beam is limited by various factors, such as the quality of services and the level of multi-use interferences. Among these, security should be of high priority, since, without it, the UEs lack privacy. The interpretation of sensitive data can cause a very significant loss. To be future proof, we reserve a security constraint on the number of served UEs per beam. Since the scope of this work is to provide a 3D BF method, the PHY layer security is not the main focus and therefore the specific technology is not discussed in depth.

Let us consider a scenario where there are *K* UEs in a beam. The other *K*-1 UEs are attempting to cooperatively interpret the information of $UE_1$ by eavesdropping. This is the worst scenario for $UE_1$. The eavesdropping threat on $UE_1$ depends on the number of the antennas of the BS and the other *K*-1 UEs. In [48], the study of such a scenario was reported in an interference alignment setting. However, there is no interference alignment in this case and the broadcast is narrowed by BF. We consider that the constraint is related to the UE density. If the neighboring UEs within the coverage of a beam are larger than a threshold, the hostile users are determined according to the following conditions.

- The distance between this neighbor and the UE is less than a predefined value.
- The transmitted signal strength of this neighbor observed by the UE is larger than a predefined value.
- The distance between this neighbor and the paired UE is less than a predefined value.

If one or any combination of the above conditions is satisfied, the neighboring UE is considered hostile.

## 5.3 Power Saving for Forthcoming Network Scenario

5G as the forthcoming step in the development of mobile communication, will be a key component of the connected society, and will help realizing the vision of essentially unlimited information access and data sharing anywhere and anytime for anyone and anything [64].

Researches on 5G cellular networks did not leave aside the issue of power saving as it is a of paramount consideration. Power saving allows to diminish operational cost and total cost of ownership in order to facilitate network connectivity in distant areas, and to provide network access in a sustainable and resource-efficient way. Two design principles for equipment activity

are considered according to when and where to transmit for the sake of scalability, management, flexible network design that both facilitates truly load-dependent energy consumption and maximizes energy-saving possibilities.

Meanwhile the thesis's scope is to provide a 3D BF method, the power saving and its related specific key technologies to efficiently achieve energy use is not the main focus and, therefore, the specific technology is not deeply discussed. To achieve the power saving in 5G cellular networks, development technologies include advanced beamforming techniques, ultra-lean design, and separation of user-data and system-control planes on the radio interface, as well as virtualized network functionality and cloud technologies [65]. 5G networks' high efficiency can be achieved by ultra-lean radio access design which may be expressed as minimize any transmissions not directly related to the delivery of user data.

Ultra-lean design is especially important for dense deployments with a large number of network nodes and highly variable traffic conditions. The use of ultra-lean transmissions can be beneficial for all kinds of deployments, including macro deployments by enabling higher achievable data rates by reducing interference from non-user-data-related transmissions. In specific situation, for the challenges brought by rapid increase of data traffic requirements due to dense connection and high demand in 5G networks, the scheme is able to distinctively serve UEs along with BF interference mitigated. This can be achieved via narrowing the generated beam to a desired BW towards UEs according to the number of engaged AEs with aim of inter-beam interference cancellation.

# Chapter 6

# Performance Verification

The proposed IBI cancellation scheme performance was verified by considering the parameter settings listed in Table 6.1, which were selected based on LTE-A specifications [66].

Table 6.1 Simulation Parameters

| **Parameters** | **Value** |
|---|---|
| NOMA Power Allocation | 0.2 and 0.8 for a UE pair |
| Carrier frequency | 1.8 GHz |
| System Bandwidth | 20 MHz |
| FFT size | 2048 |
| Number of data carriers | 1200 |
| Number of samples in CP | 144 |
| Subcarrier spacing | 15 kHz |
| BS antenna configuration (PM-MIMO) | 1 MUX × 32 AE × 3 branches |
| BS AE spacing | Half wavelength |
| User's antenna configuration | 1 AE × 3 branches |
| Radius of user's local area ($r_{UE}$) | 15 m |
| Antenna type | Dipole |
| Modulation | QPSK |
| Number of scatterers | Outdoor: 4 clusters with 16 scatterers per cluster (64 in total) |
| Scattering sphere radius | 10 m |
| Velocity of users | 3, 60, and 120 km/h |
| Fading | Flat |
| XPD value | 5.8 dB |
| Correlation | 0.32 |

In this study, we considered a downlink single cell, and used the downlink data mapping based on the LTE-A type of resource blocks, as shown in Fig. 10 in [56]. Figure 6.1 clarifies

the performance of the proposed IBI cancellation scheme shown in Figure 5.3, which demonstrates the scheme's robustness in the process of IBI cancellation by keeping the required BW. The BW variation according to the proposed scheme and the cumulative distribution functions (CDF) of the simulation engendered HPBW are depicted in Figure 6.1. It is clearly shown that the average HPBW is brought to about 20° for different steps in HPBW. The variation in user density shows the respective change in the performance curves at 50% of the CDF value, that is, for respective values of $\lambda$ of 14, 16, and 18. The robustness of the proposed IBI cancellation scheme can then allow the optimization of the generated BW to eliminate BF interference.

The evaluation of the spectrum efficiency of the proposed scheme depicted in Figure 6.2, with low $\lambda$ values, e.g., $\lambda = 4$, shows that the performance gain of the proposed IBI cancellation scheme is comparatively small because of low interference and leads to the proposed scheme's efficiency being low for such values. For example, at a target SNR of 30 dB, the proposed IBI cancellation obtains only a 4 bits/s/Hz gain.

Increasing the UE density to $\lambda = 8$, the performance gain is increased because of the proposed IBI cancellation scheme, and its performance results lead toward interference reduction, e.g., about a 9 bits/s/Hz gain is achieved. Again, for a higher $\lambda = 12$, the performance decreases.

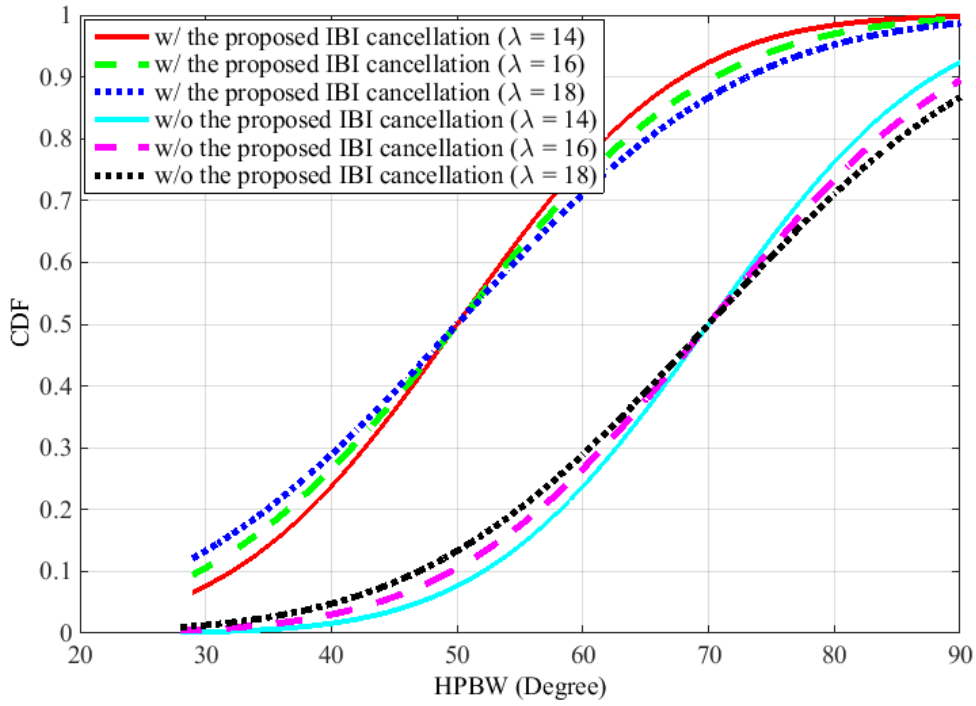


Figure 6.1 Cumulative distribution function of half power beam-width.

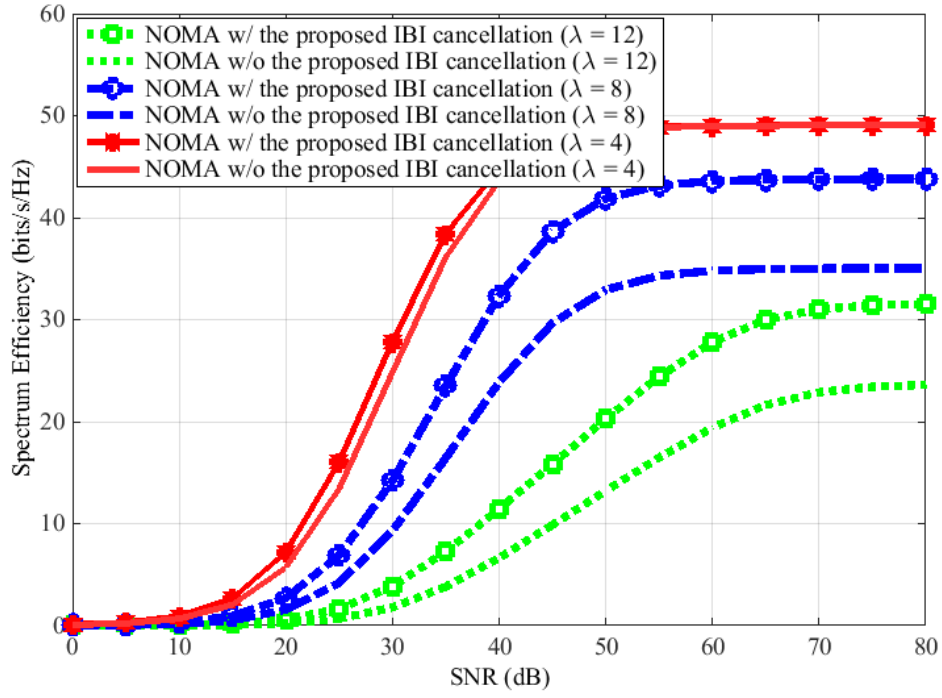


Figure 6.2 Spectrum efficiency for different user densities.

This is caused by the limited number of AEs, which leads to a non-optimally narrowed BW. For each considered UE density case, the spectrum efficiency performance positively and distinctively increases, which indicates the valuableness and consistency of the proposed scheme.

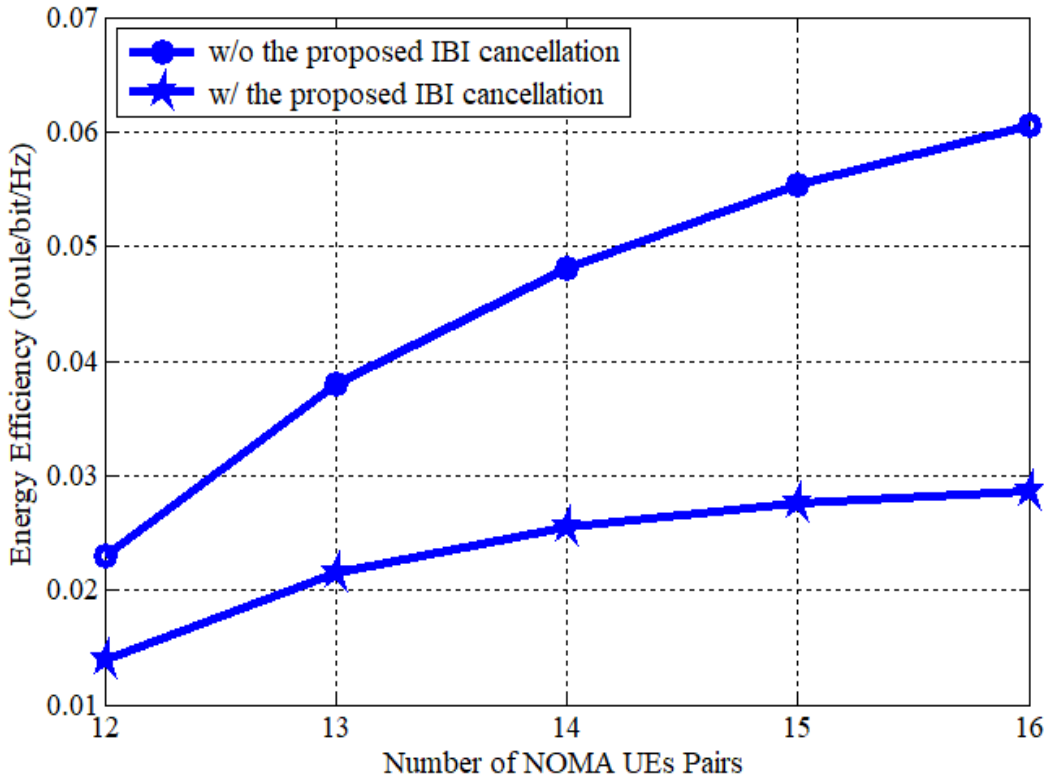


Figure 6.3 Energy efficiency with respect to the number of NOMA UEs pairs.

The proposed IBI cancellation scheme shows the best performance on power saving, of which the energy efficiency increases with an increase in the number of NOMA UEs pairs as shown in Figure 6.3. The performance in power saving is evaluated and exemplified by

achieving a rate of 0.032 joule/bit/Hz for 16 NOMA UEs pairs. In the same way, Figure 6.4 shows the performance of the proposed IBI cancellation scheme with consideration of different user densities where the achieved energy efficiency can be evaluated to 0.0395 joule/bit/Hz for $\lambda = 4$. The proposed scheme shows that energy efficiency in a cell increases with an increase in the number of users.

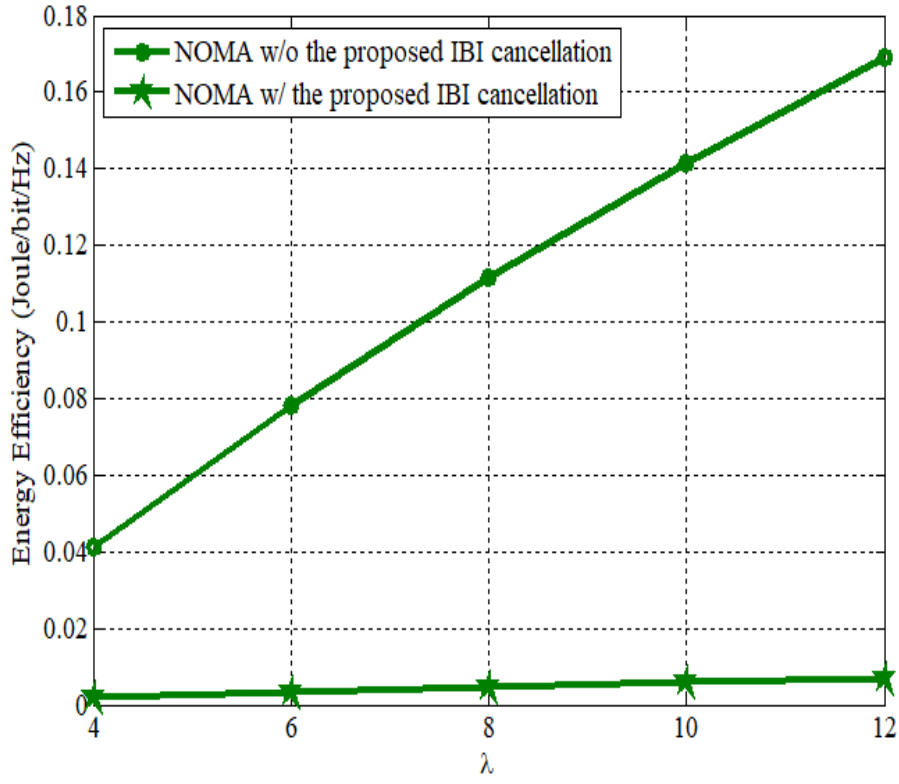


Figure 6.4 Energy efficiency with respect to user density ($\lambda$).

# Chapter 7

# Conclusions

In this thesis, a downlink single cell is considered and evaluated by the performance of a NOMA system with the proposed scheme in the IBI cancellation process. According to NOMA attributes, many studies have been conducted on NOMA combined with other technologies, such as massive MIMO, and BF technologies that may be capable of meeting 5G requirements. In addition, because interference is one of the hindrances to cellular wireless communication, a scheme that enhances the practicability of a power domain NOMA system by using a 3D polarized BF in the process of IBI cancellation was proposed. The proposed scheme improves the system spectrum efficiency as well as energy efficiency. Based on the BS antenna configuration, with the proposed scheme, an appropriate number of AEs is required to suitably narrow the generated beam to the desired BW. With the proposed scheme, the average HPBW is brought to about 20° for different steps in HPBW and different UE densities. The robustness of the proposed IBI cancellation scheme can then allow optimization of the generated BW to eliminate BF interference.

In the spectrum efficiency evaluation, the performance gain was shown to be comparatively small when UE density is low, e.g., $\lambda = 4$, because of low interference. At a target SNR of 30 dB, the proposed IBI cancellation obtains only a 4 bits/s/Hz gain. When the UE density is increased to $\lambda = 8$, the performance gain as a result of the proposed IBI cancellation scheme increases and its performance leads to interference reduction, where a spectrum efficiency of about 9 bits/s/Hz gain is achieved. For higher UE density, e.g., $\lambda = 12$, the performance

decreases. This is caused by the limited number of AEs, which leads to a non-optimally narrowed BW.

By applying the proposed scheme in the process of IBI cancellation, the spectrum efficiency performance is positively and distinctively increased for each considered UE density case, which indicates the valuableness and consistency of the proposed scheme. The proposed IBI cancellation scheme also shows the best performance on power saving, of which the energy efficiency increases with an increase in the number of NOMA UEs pairs as well as user density within a cell.

# References


[1] Z. Ding, “Application of non-orthogonal multiple access in LTE and 5G networks,” *IEEE Communication Magazine*, vol. 55, no. 2, pp. 185-191, Feb. 2017.

[2] J. Cui, Z. Ding, and P. Fan, ‘‘A novel power allocation scheme under outage constraints in NOMA systems,’’ *IEEE Signal Processing Letters*, vol. 23, no. 9, pp. 1226 - 1230, Sept. 2016.

[3] R. Vannithamby, and S. Talwar, *Towards 5G: Applications, requirements and candidate technologies*, John Wiley & Sons, Ltd, United Kingdom, 1st edition, 472 pages, 2017.

[4] V. W. S. Wong, R. Schober, D. W. K. Ng, and L.-C. Wang, *Key Technologies for 5G Wireless Systems*, Cambridge university Press, United Kingdom, 1st edition, pp. 110-111, 2017.

[5] X. Liu and X. Wang, “Efficient antenna selection and user scheduling in 5G massive MIMO-NOMA system,” in *Proc. IEEE Vehicular Technology Conference (VTC Spring)*, July 2016, pp. 1-5.

[6] Z. Ding and H. V. Poor, “Design of massive-MIMO-NOMA with limited feedback,” *IEEE Signal Process. Lett.*, vol. 23, no. 5, pp. 629-633, May 2016.

[7] Z. Ruan, Y. Miao, L. Pan, N. Patterson, and J. Zhang, “Visualization for big data security – A case study on KDD99 cup data set,” *Digital Communications and Networks* (2017), doi: 10.1016/j.dcan.2017.07.004.

[8] S.K. Bhoi, P.M. Khilar, M. Singh, R.R. Sahoo, and R.R. Swain, “A routing protocol for urban vehicular ad hoc networks to support non-safety applications,” *Digital Communications and Networks* (2017), doi: 10.1016/j.dcan.2017.08.003.

[9] Z. Guan, and G. Si, "Achieving privacy-preserving big data aggregation with fault tolerance in smart grid," *Digital Communications and Networks* (2017), doi: 10.1016/j.dcan.2017.08.005.

[10] A. Li, A. Harada, and H. Kayama, "Investigation on low complexity power assignment method and performance gain of non-orthogonal multiple access systems," *IEICE Transactions on Fundamentals of Electronics, Communications and Computer Sciences*, vol. E97-A, no.1, pp. 57-68, Jan. 2014.

[11] Y. Saito, A. Benjebbour, Y. Kishiyama, and T. Nakamura, "System level performance evaluation of downlink non-orthogonal multiple access (NOMA)," in *IEEE* Personal Indoor and Mobile Radio Communications (*PIMRC) 2013*, Sept. 2013, pp. 1-5.

[12] Y. Liu, G. Pan, H. Zhang, and M. Song, "On the capacity comparison between MIMO-NOMA and MIMO-OMA," *IEEE Access*, vol. 4, pp. 2123-2129, May 2016.

[13] X. Chen, A. Benjebbour, Y. Lan, A. Li, and H. Jiang, "Impact of rank optimization on downlink non-orthogonal multiple access (NOMA) with SU-MIMO," *IEEE International Conference on Communication Systems (ICCS), 2014*, pp. 1-5, Nov. 2014.

[14] X. Wei, H. Liu, Z. Geng, et al., "Software defined radio implementation of a non-orthogonal multiple access system towards 5G," *IEEE Access*, vol. 4, pp. 9604 - 9613, Jan. 2017.

[15] NTT DOCOMO, "Requirements, candidate solutions & technology roadmap for LTE rel-12 onward," *3GPP RWS-120010*, June 2012, 27 pages.

[16] Y. Kishiyama, A. Benjebbour, H. Ishii, and T. Nakamura, "Evolution concept and candidate technologies for future steps of LTE-A," *IEEE Int. Conf. on Comm. Syst. (ICCS2012)*, pp. 473-477, Nov. 2012.

[17] H. Lee, S. Kim, and J. H. Lim, ‘‘Multiuser superposition transmission (MUST) for LTE-A systems,’’ in *Proc. IEEE Int. Conf. Commun. (ICC)*, pp. 1-6, May 2016.

[18] Z. Wei, J. Yuan, D. W. K. Ng, M. Elkashlan, and Z. Ding, “A survey of downlink non-orthogonal multiple access for 5G wireless communication networks,” ZTE Commun., vol. 14, no. 4, pp. 17-25, Oct. 2016.

[19] S. M. R. Islam, M. Zeng, and O. A. Dobre, “NOMA in 5G systems: exciting possibilities for enhancing spectral efficiency,” *IEEE 5G Tech Focus*, vol. 1, no. 2, pp. 1-6, June 2017.

[20] H. Mehrpouyan, M. R. Khanzadi, M. Matthaiou, A. M. Sayeed, R. Schober, and Y. Hua, “Improving bandwidth efficiency in E-band communication systems,” *IEEE Communications Magazine*, vol. 52, no. 3, pp. 121-128, Mar. 2014.

[21] S. M. R. Islam, N. Avazov, O. A. Dobre, and Kyung-sup Kwak, ‘‘Power-domain non-orthogonal multiple access (NOMA) in 5G systems: Potentials and challenges,’’ *IEEE Communications Surveys and Tutorials,* vol. 19, Issue no. 2, pp. 721 – 742, Oct. 2016.

[22] H. Tabassum, M.S. Ali, E Hossain, M. Hossain, and D.I. Kim, ‘‘Non-orthogonal multiple access (NOMA) in cellular uplink and downlink: challenges and enabling techniques,’’ arXiv preprint arXiv:1608.05783, pp. 1-8, Aug. 2016.

[23] L. Dai, B. Wang, Y. Yuan, S. Han, C.-L. I, and Z. Wang, ‘‘Non-orthogonal multiple access for 5G: Solutions, challenges, opportunities, and future research trends,’’ *IEEE Communications Magazine*, vol. 53, no. 9, pp. 74 – 81, Sept. 2015.

[24] X. M. Hong, Y. Jie, C. X. Wang, J. H. Shi, and X. H. Ge, “Energy-spectral efficiency trade-off in virtual MIMO cellular systems,” in *IEEE Journal on Selected Areas in Communications*, vol. 31, no. 10, pp. 2128-2140, Oct. 2013.

[25] X. H. Ge, T. Han, Y. Zhang, G. Q. Mao, C. X. Wang, J. Zhang, B. Yang, and S. Pan, "Spectrum and energy efficiency evaluation of two-tier femtocell networks with partially open channels," in *IEEE Transactions on Vehicular Technology*, vol. 63, no. 3, pp. 1306-1319, Mar. 2014.

[26] H. Osada, M. Inamori, and Y. Sanada, "Non-orthogonal access scheme over multiple channels with iterative interference cancellation and fractional sampling in MIMO-OFDM receiver," in *Proc. of IEEE Vehicular Technology Conference (VTC Fall)*, pp. 1-5, Sept. 2013.

[27] K. Saito, et al., "Link-level performance of downlink NOMA with SIC receiver considering error vector magnitude," in *Proc. of IEEE Vehicular Technology Conference (VTC Spring)*, pp. 1-5, May 2015.

[28] H. Haci, and H. Zhu, "Performance of non-orthogonal multiple access with a novel interference cancellation method," in *Proc. of IEEE International Conference on Communications (ICC)*, pp. 2912-2917, June 2015.

[29] P. Li, R. D. De Lamare, and R. Fa, "Iterative successive interference cancellation based on multiple feedback for multiuser MIMO systems," in *Wireless Conference - Sustainable Wireless Technologies*, pp. 1-6, Apr. 2011.

[30] B. Knoop, F. Monsees, C. Bockelmann, D. Wuebben, S. Paul, and A. Dekorsy, "Sparsity-aware successive interference cancellation with practical constraints," in *17th International ITG Workshop on Smart Antennas (WSA)*, pp. 1-8, Mar. 2013.

[31] M. Mandloi, M. A. Hussain, and V. Bhatia, "Improved multiple feedback successive interference cancellation algorithm for near-optimal MIMO detection," in *IET Communications*, vol. 11, no. 1, pp. 150-159, Dec. 2016.

[32] X. Xu, and N. Goertz, “Practical successive interference cancellation in the binary-input gaussian multiple-access channel,” in *7th International ITG Conference on Source and Channel Coding (SCC)*, pp. 1-6, Jan. 2008.

[33] M. Morelli, and U. Mengali, “A comparison of pilot-aided channel estimation methods for OFDM systems,” in *IEEE Transactions on Signal Processing*, vol. 49, no. pp. 3065-3073, Dec. 2001.

[34] A. R. Varma, C. R. N. Athaudage, L. L. H. Andrew, and J. H. Manton, “Optimal superimposed pilot selection for OFDM channel estimation,” in *Proc. of IEEE SPAWC*, pp. 1-5, July 2006.

[35] X. Su, H. F. Yu, K. H. Chang, S. G. Kim, and Y. K. Lim, “Case study for ship ad-hoc networks under a maritime channel model in coastline areas,” in *KSII Transactions on Internet and Information Systems*, vol. 9, no. 10, pp. 4002-4014, Oct. 2015.

[36] F. Uddin, and S. Mahmud, “Carrier sensing-based medium access control protocol for WLANs exploiting successive interference cancellation,” in *IEEE Transactions on Wireless Communications*, vol. 16, no. 6, pp. 4120-4135, Apr. 2017.

[37] B. Kim, S. Lim, H. Kim, et al., “Non-orthogonal multiple access in a downlink multiuser beamforming system,” in *Proc. of IEEE Military Communications Conferences (MILCOM)*, pp. 1278-1283, Nov. 2013.

[38] A. Li, A. Benjebbour, and A. Harada, “Performance evaluation of non-orthogonal multiple access combined with opportunistic beamforming,” in *Proc. of IEEE Vehicular Technology Conference (VTC Spring)*, pp. 1-5, May 2014.

[39] K. Higuchi and Y. Kishiyama, “Non-orthogonal access with random beamforming and intra-beam SIC for cellular MIMO downlink,” in *Proc. of IEEE Vehicular Technology Conference (VTC Fall)*, pp. 1-5, Sept. 2013.

[40] Y. Hayashi, Y. Kishiyama, and K. Higuchi, “Investigations on power allocation among beams in non-orthogonal access with random beamforming and intra-beam SIC for cellular MIMO downlink,” in *Proc. of IEEE Vehicular Technology Conference (VTC Fall)*, pp. 1-5, Sept. 2014.

[41] Y. Jinhong, X. Jiying, D. Zhiguo, and Y. Zhifeng, **‘‘**Multiple access techniques for 5G**,’’** *ZTE Communications*, Special Topic, vol.14, no. 4, pp. 1-2, Oct. 2016.

[42] R. C. Kizilirmak, and H. K. Bizaki ‘‘Non-orthogonal multiple access (NOMA) for 5G networks,’’ *Towards 5G Wireless Networks - A Physical Layer Perspective*, InTech, 242 pages, Dec. 2016, doi: 10.5772/63098.

[43] Z. Ding, F. Adachi, and H. V. Poor, “The application of MIMO to non-orthogonal multiple access,” *IEEE Trans. Wireless Commun.*, vol. 15, no. 1, pp. 537–552, 2016.

[44] Q. Sun, S. Han, C.-L. I, and Z. Pan, “On the ergodic capacity of MIMO NOMA systems,” *IEEE Wireless Communications Letters*, vol. 4, no. 4, pp. 405–408, 2015.

[45] Z. Yang, Z. Ding, P. Fan, and G.K. Karagiannidis, ‘‘On the performance of non-orthogonal multiple access systems with partial channel information,’’ *IEEETrans. Comm*., vol. 64, no. 2, pp. 654-667, 2016.

[46] Y. Liu, H.-H. Chen and W. Min, “Physical layer security for next generation wireless networks: Theories, technologies, and challenges”, *IEEE Communication Surveys and Tutorials*, vol.19, no.1, pp. 347-375, First quarter 2017.

[47] W. Fang, F. Li, Y. Sun and et. al., “Information security of PHY layer in wireless networks”, *Journal of sensor*, vol. 2016, page 10.

[48] N. Zhao, F. Richard Yu, Ming Li, Qiao Yan, and Victor C. M. Leung, “Physical layer security issues in interference-alignment-based wireless networks,” *IEEE Communications Magazine*, ， pp.162-168, Aug. 2016.

[49] Y. Zhang, H. M. Wang, Q. Yang and Z. Ding, “Secrecy sum rate maximization in non-orthogonal multiple access,” in *IEEE Communications Letters*, vol. 20, no. 5, pp. 930-933, May 2016.

[50] Y. Liu, Z. Qin, M. Elkashlan, Y. Gao and L. Hanzo, “Enhancing the physical layer security of non-orthogonal multiple access in large-scale networks,” in *IEEE Transactions on Wireless Communications*, vol. 16, no. 3, pp. 1656-1672, March 2017.

[51] Q. Bi, L. Liang，S. Yang，and C. Peng, “Non-orthogonal multiple access technology for 5G Systems,” *Telecommunications Science, 2015 137*, pp. 2-3, May 2015.

[52] Y. Saito, Y. Kishiyama, A. Benjebbour, T. Nakamura, A. Li, and K. Higuchi, “Non-orthogonal multiple access (NOMA) for cellular future radio access,” in *Proc. of IEEE Vehicular Technology Conference (VTC Spring)*, pp. 1-5, June 2013.

[53] X. Li, L. Li, F. Wen, J. Wang, and C. Deng, “Sum rate analysis of MU-MIMO with a 3D MIMO base station exploiting elevation features,” *International Journal of Antennas and Propagation* Volume 2015, Article ID 318123, 9 pages.

[54] J. G. Andrews, R. K. Ganti, A. M. Haenggi, N. Jindal, and S. Weber, “A primer on spatial modeling and analysis in wireless networks,” *IEEE Communications Magazine*, Nov. 2010, 10 pages.

[55] A. D. Panagopoulos, "Handbook of research on next generation mobile communication systems, *Advances in wireless technologies and telecommunication*," IGI Global, 152 pages, 2015.

[56] X. Su and K. H. Chang, "Diversity and multiplexing technologies by 3D beams in polarized massive MIMO systems," *Mobile Information Systems*, vol. 2016, Article ID 2318287, 15 pages, 2016.

[57] X. Su and K. H. Chang, "Polarized uniform linear array system: Beam radiation pattern, beamforming diversity order, and channel capacity," *International Journal of Antenna and Propagation*, vol. 2015, Article ID 371236, 9 pages, 2015.

[58] S. F. Maharimi, M. F. Abdul Malek, M. F. Jamlos, S. C. Neoh, and M. Jusoh, "Impact of spacing and number of elements on array factor," in *Proc. PIERS*, pp 1150-1553, Mar. 2012.

[59] O. N. C. Yilmaz, S. Hämäläinen, and J. Hämäläinen, "System level analysis of vertical sectorization for 3GPP LTE," in *Proc. IEEE Conf. ISWCS*, pp. 453-457, Sep. 2009.

[60] M. Caretti, M. Crozzoli, G. M. Dell'Aera, and A. Orlando, "Cell splitting based on active antennas: Performance assessment for LTE system," in *Proc. IEEE Conf. WAMICOM*, pp. 1-5, Apr. 2012.

[61] H. Huang, O. Alrabadi, J. Daly, D. Samardzija, C. Tran, and R. Valenzuela, "Increasing throughput in cellular networks with higher-order sectorization," in *Proc. Asilomar Conf. Signal, Systems, and Computers*, pp. 630-635, Nov. 2010.

[62] C.-S. Lee, M.-C. Lee, C.-J. Huang, and T.-S. Lee, "Sectorization with beam pattern design using 3D beamforming techniques," in *Proc. APSIPA ASC*, PID 2928677, 5 pages, Oct. 2013.

[63] J. Litva and T. K. Lo, *Digital Beamforming in Wireless Communications*, Artech House, 1st edition, 320 pages, 1996.

[64] Ericsson, Feb. 2015, White paper: 5G radio access – technology and capabilities, available at: http://www.ericsson.com/res/docs/whitepapers/wp-5g.pdf

[65] Ericsson, Apr. 2016, White paper: 5G technology components, Uen 284 23-3204 Rev C.

[66] ETSI TS 136 211 v12.7.0 (2015-10), "LTE evolved universal terrestrial radio access (E-UTRA), physical channels and modulation," Technical Specification, 2015.